Spring 2015

Dielectric coating of iron particles by electrostatic colloidal deposition

Daniel Kim
Purdue University

Graduate School Form 30
Updated 1/15/2015

PURDUE UNIVERSITY
GRADUATE SCHOOL
Thesis/Dissertation Acceptance

This is to certify that the thesis/dissertation prepared

By Daniel Kim

Entitled
DIELECTRIC COATING OF IRON PARTICLES BY ELECTROSTATIC COLLOIDAL DEPOSITION

For the degree of Master of Science in Materials Science Engineering

Is approved by the final examining committee:

Kevin P. Trumble
Co-chair

Jeffrey P. Youngblood
Co-chair

Elliott B. Slamovich

To the best of my knowledge and as understood by the student in the Thesis/Dissertation Agreement, Publication Delay, and Certification Disclaimer (Graduate School Form 32), this thesis/dissertation adheres to the provisions of Purdue University's "Policy of Integrity in Research" and the use of copyright material.

Approved by Major Professor(s): Kevin Trumble

Approved by: David Bahr 4/23/2015
Head of the Departmental Graduate Program Date

DIELECTRIC COATING OF IRON PARTICLES BY ELECTROSTATIC COLLOIDAL DEPOSITION

A Thesis

Submitted to the Faculty

of

Purdue University

by

Daniel Kim

In Partial Fulfillment of the

Requirements for the Degree

of

Master of Science in Materials Engineering

May 2015

Purdue University

West Lafayette, Indiana

For my family

Thank my parents for giving me the opportunity to study in Purdue University. You guys always helped me with support and love during my life in U.S.A. Also, I thank my sister for providing me advice and you are a person that I always admire. I love my family and I send my best wishes for their continued health.

ACKNOWLEDGEMENTS

I would like to express my appreciation to my two advisors, Professor Kevin Trumble and Professor Jeffery Youngblood. They all went on sabbatical in my first year in Purdue University, but they always helped me with their advice and support. My gratitude also goes to Professor Elliot Slamovich and Professor Mysore Dayananda. When my two main advisors were on sabbatical, they helped me no matter how busy they were. Thanks to Dr. Patti Metcalf for providing guidance in the beginning of my research. Also, thanks to GKN Hoeganaes Corporation for the financial support of this study.

TABLE OF CONTENTS

Page

LIST OF TABLES

Table Page

LIST OF FIGURES

Figure Page

ABSTRACT

Kim, Daniel. M.S.M.S.E., Purdue University, May 2015. Dielectric Coating of Iron Particles by Electrostatic Colloidal Deposition: Major Professors: Kevin Trumble and Jeffery Youngblood.

Iron is a soft magnetic material widely used in electric motors, generators, and transformers because they demand high permeability and low core loss. The main goal of this project is to develop a commercially viable coating of iron powders for press-and-sinter processing that would enable higher firing temperatures to anneal out magnetic defects, while maintaining high electrical resistivity (~10,000 μΩ-cm) and high iron density (>90 %). An alumina-modified colloidal silica (LUDOX CL), was used in early work to make Fe (-)/SiO_2 (+) in a wet-pressed route. The highest relative density and resistivity measurements for a wet-pressing route were 87 % and 7300 ± 1000 μΩ-cm respectively. Dry-pressed route is favorable over wet-pressed route because it can be commercially viable. About 100-fold increase in resistivity (860,000 μΩ-cm) was obtained compared to the wet-pressed route, with only a small decrease in density (1 – 2 %). A study was conducted to explore the separate, and possibly interactive, effects of micro-alumina particulate (Sumitomo AKP-50, 0.2 μm) and lubricant (Kenolube, a proprietary metal soap-wax composite lube). Reducing the LUDOX CL, high shear

mixing using a coffee grinder, and multimodal packing were studied to improve density. Only 10 % reduction of LUDOX CL dropped the resistivity by over two orders of magnitude with the same relative density. High shear mixing and multimodal packing had little effects to increase density. An unmodified colloidal silica (LUDOX TM) was also explored to make Fe (+) /SiO_2 (-) and resistivity of 120,000 μΩ-cm and 80 % density were obtained. Addition of cationic polyelectrolyte, polydiallyldimethyl-ammonium chloride (PDADMAC) was studied to provide stronger adhesion between LUDOX TM and surface of iron particles. Reducing the amount of LUDOX TM in PDADMAC showed relative density greater than 90 % but resistivity measurements were less than 1500 μΩ-cm.

CHAPTER 1. INTRODUCTION

Iron is the fourth most abundant element on Earth and the most widely used metal, due mainly to its low cost. According to U.S Geological Survey (USGS) 53 million tons of all types of ferrous scrap was consumed in the US in 2012 at value of 19.9 billion dollars [1]. Besides large production/consumption and low cost, iron possesses many desirable properties such as ductility, ability to strengthen by alloying, and magnetic properties [2]. Among them, the ferromagnetic properties are of primary interest in this study.

Iron is classified as soft magnetic materials which can be easily magnetized and demagnetized. In general, it has intrinsic coercive force less than 10 A/cm. Iron is extensively used for high permeability and low core loss. The most commonly used soft magnetic material at low frequency (60-200 Hz) is lamination steel due to its design ease, low cost, and sufficient magnetic properties [3]. However, the laminated thin sheets with insulator between limit the eddy current losses to two-dimensional flux and this is a crucial limitation for minimizing eddy current losses at high frequency [3]. Coating particles with insulating materials provide a key for three-dimensional magnetic flux because of ability to process in complex shapes by Powder Metallurgy (P/M). It is called soft magnetic composites (SMC). They are prepared by coating of ferromagnetic particles

with insulating materials and then followed by P/M methods involving pressing and annealing [4]. Another advantage of SMCs is lowering core loss. Core loss is composed of two primary sources, hysteresis and eddy current losses. Hysteresis loss is from the difficulty of magnetic domain wall switching. It is due to strain (dislocations) from plastic deformation at particle contacts in die pressing and it is a dominant factor in core loss at low frequency [5]. High temperature annealing can relieve strain, thus lowering hysteresis loss, increasing mechanical strength and previous work indicated that annealing increases permeability as well [5]. Eddy current loss is generated by heat associated with magnetic field changes. It can be minimized by increasing resistivity but the biggest drawback of pure iron (a minimum of 99.8 % purity) is its low resistivity (~10 $\mu\Omega \cdot$cm at room temperature) [6]. Thus, the insulating coating in SMCs provides a key to decrease eddy current loss. However, insulating coating of iron particles lowers permeability due to the gap created between particles and the reduced amount of metal in the system [6]. In order to obtain high permeability, high density in the system is required.

In this work, SMC processing methods were developed to produce a commercially viable coating of iron powder for press-sinter processing that would enable higher firing temperatures to anneal out magnetic defects, while maintaining high electrical resistivity (~10,000 $\mu\Omega$-cm) and iron density (> 90 %).

CHAPTER 2. BACKGROUND

2.1 P/M Iron Soft Magnetic Materials

There are great interests in Powder Metallurgy (P/M) for materials that exhibit magnetic properties because of the ability to process in complicated shapes with low cost. P/M processes can be divided into two major categories; compaction-based densification and sintering-based densification, shown in Figure 1 [2].

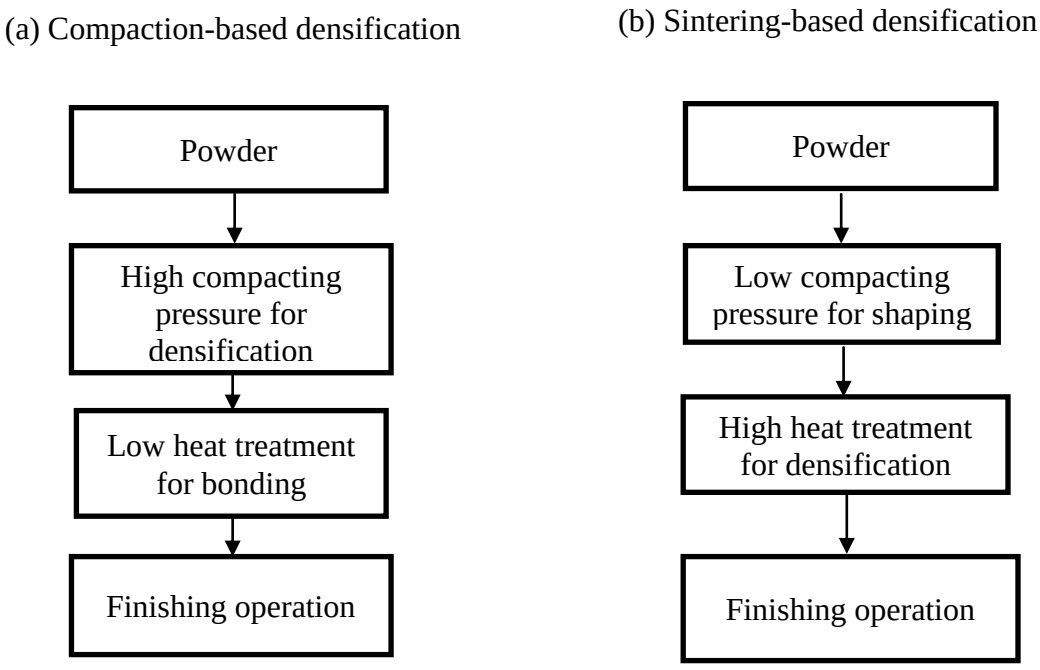

Figure 1**.** A schematic of P/M processes, compaction-based and sintering-based densification [2].

Most densification takes place in pressing for compaction-based densification. Sintering is a step to bond the particles so it requires high compacting pressure and low sintering temperature [2]. Sintering-based densification is opposite, where densification occurs in sintering [2]. It requires low compacting pressure for shaping and high sintering temperature. Also, there is a combination of these two processes, hybrid densification, which apply pressure and temperature simultaneously [2]. Compacting pressure and temperature are two major components to consider since they affect magnetic properties. Compacting in high pressure results in increasing density but plastic deformation is known to degrade magnetic properties due to residual stresses and interaction of domain walls and dislocations [7].

Materials can be categorized as hard or soft materials depending on hysteresis characteristics. Hysteresis term is originated from the Greek word, hysterein, meaning "to lag behind" [4]. This effect is produced when magnetic flux density (B) does not return along the same curve and lags behind the applied magnetic field strength (H). The remanence, denoted as B_r, describes a residual B field at zero H field. Coercivity (H_c), also coercive force, describes reverse H field needed to reduce the B field to zero. As shown in Figure 2, further increasing H field in the opposite direction yields saturation in the reverse [8]. Thus, second reverse of the field to initial saturation completes the loop.

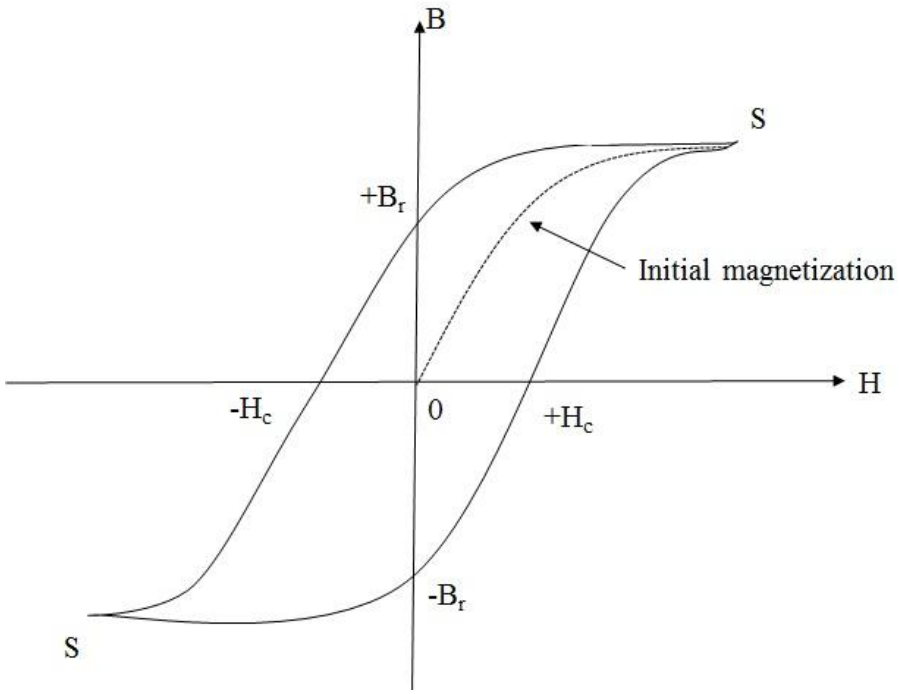

Figure 2. The hysteresis loop of ferromagnetic material showing magnetic flux density (B) versus magnetic field strength (H): solid curve is hysteresis loop and the dashed curve shows initial magnetization [8].

With soft magnetic materials the hysteresis loop is very narrow (low coercive force < 10 A/cm) and with hard magnets the hysteresis loop is very wide (high coercive force > 100 A/m), shown in Figure 3 [9]. Advantages of soft magnetic materials are that they are easily magnetized and demagnetized corresponding to low core loss [10]. They can also have high permeability, a magnetic sensitivity representing a ratio of flux density to magnetizing force, and low coercive force.

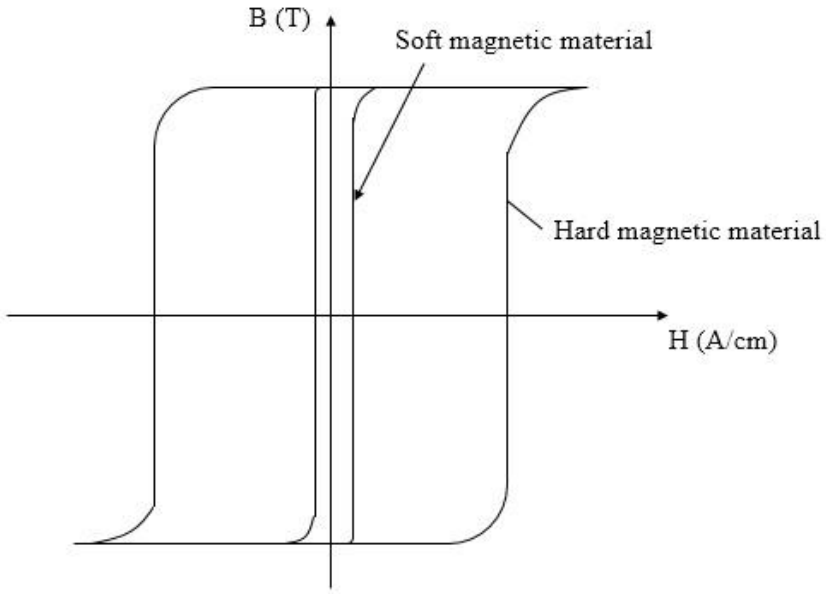

Figure 3. Magnetization curves for soft and hard magnetic materials [9].

Some of examples of iron soft magnetic materials from P/M processes are pure iron and a few simple alloys, including Fe-2Ni, Fe-3Si, Fe-0.45P, Fe-0.6P, and Fe-50Ni [2]. Table 1 compares the magnetic properties of typical P/M alloys. Fe-50Ni alloy possesses higher permeability and lower coercive force compared to other alloys.

Table 1. Magnetic properties of typical P/M alloys [2].

Alloy	Resistivity (μΩ-cm)	Maximum magnetization (T)	Remanence magnetization (T)	Coercive force (Oe)	Maximum relative permeability
Fe	20	1.6	1.2	1.4	4000
Fe-49Co-2V	40	2.0	5.6	3.0	3000
Fe-50Co	60	1.7	0.56	2.0	2000
Fe-50Ni	40	1.3	0.9	0.3	25000
Fe-0.45P	21	1.4	1.2	1.1	4000
Fe-0.8P	23	1.8	1.3	0.4	6100
Fe-3Si	45	1.4	1.3	0.9	4500
Fe-6.5Si	81	1.3	1.2	0.3	4000

Hysteresis loss is one component in core loss. Hysteresis loss dominates at low frequency (< 200 Hz) and it is expressed as the following [11]:

$$W_H = K_H * Loop\ area * f \qquad (1)$$

Where W_H (W/kg) is hysteresis loss, K_H is hysteresis constant and f (Hz) is frequency. It is created when magnetic energy is converted to heat that dissipates into the lattice and can raise temperature. In soft magnetic materials, hysteresis loss is very undesirable because of further problems in devices, created by heat associated with it.

The other component of core loss is eddy current loss, which dominates at high frequency. Eddy current is generated in the core from electrical currents when magnetic field changes [11]. It creates unwanted heat within the core materials. Eddy current loss can be expressed as the following [11]:

$$W_E = K_E * \frac{d*B^2*f^2}{\rho} \qquad (2)$$

where W_E(W/kg) is eddy current loss, K_E is an eddy loss constant, d (mm) is the thickness, B (T) is the induction level, f (Hz) is the frequency and ρ (μΩ-m) is the resistivity of material. Eddy current loss depends on frequency (f) to the power of two compared to the power of one in hysteresis loss, showing that hysteresis loss is dominant at low and eddy current loss is dominant at high frequencies. Eddy current loss can be categorized in inter-particle and intra-particle eddy current losses, shown in Figure 4.

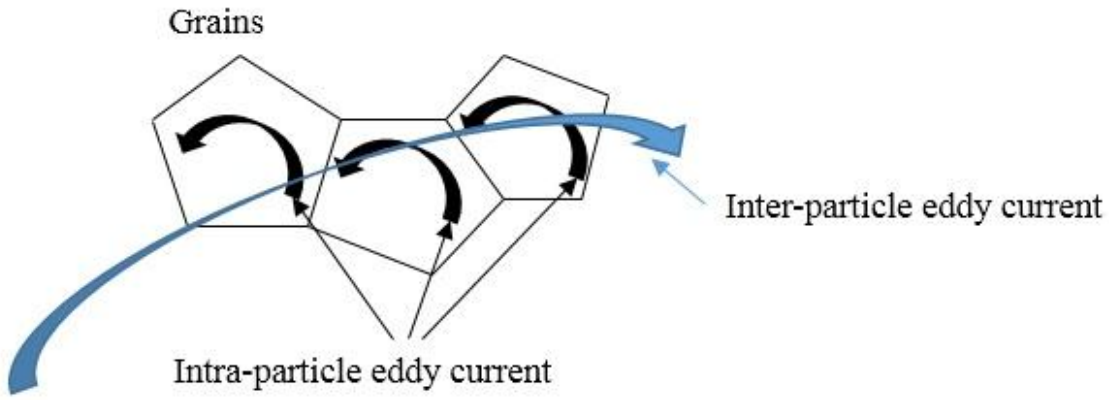

Figure 4. A schematic of inter-particle and intra-particle eddy current.

If one assumes that insulation between particles is perfect, the system will have only intra-particle eddy current losses [12]. However, high compacting pressure from P/M process often creates fractures in insulation. This increases inter-particle eddy current loss. Thus, more generalized total eddy current loss equation can be obtain as the following [3]:

$$W_{TE} = (K_{E1} * B^2 * f^2) + (K_{E2} * \frac{d*B^2*f^2}{\rho}) \qquad (3)$$

where W_{TE} (W/kg) is total eddy current loss, K_{E1} is inter-particle eddy current constant and K_{E2} is intra-eddy current constant. The first term describes inter-particle eddy current loss and second term describes intra-particle eddy current loss. Eddy currents are also known to decrease the permeability in AC field. Eddy current circulates in a direction opposing to the applied magnetic field so high eddy current is likely to reduce magnetic field in the core [11]. Eddy current loss can be minimized by increasing resistivity of material. This can be done with insulating coating on particles or solid solution alloying, although this reduces permeability also. Current commercial processes to coat iron powder with insulating materials will be discussed in the next section.

2.2 Current Commercial Processes

Here, current commercial processes are described [13]. They include fluid-bed powder coating, conventionally compacted coating, and annealed coating. Detailed description of each process will be discussed.

2.2.1 Fluid-bed Powder Coating

Fluid bed processing can be used in a variety of applications such as drying, agglomeration/ granulation, and powder coating [14]. There are three types of fluid-bed processes and they are characterized by position of spraying nozzle; top (top spray), bottom (bottom spray), or side (tangential spray), shown in Figure 5 [15]. Different types of fluid-bed processes can be selected depending on the applications. For example, top and tangential spray fluid-bed are widely used processes for granulation, but all three types of fluid-bed processes can be used in powder coating process. Common processing conditions involve passing a gas to create a fluidized state. Bottom spray fluid bed process is the most commonly used process for coating because of unique features like cylindrical partition in chamber and configuration of air dispenser plate, allowing short distance between particles and coating materials [15]. This is beneficial to limit spray-drying to produce uniform coated particles.

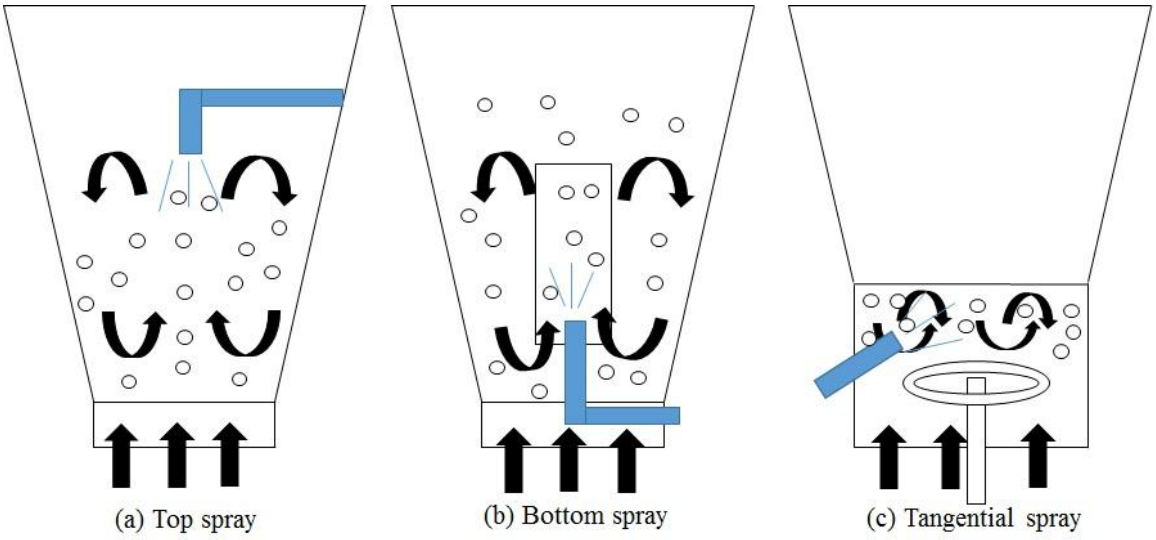

Figure 5. Three types of fluid-bed coating process; (a) top spray, (b) bottom spray, (c) tangential spray [15].

Material and finished part production process of pressed iron powder reviewed by Hoegaenes Company [13] is shown in Figure 6. The iron powder in fluid-bed coating process is coated with approximately 0.5 to 1.0 wt % non-conductive polymer. Then, the warm compaction process is followed to produce high density and strength compacts.

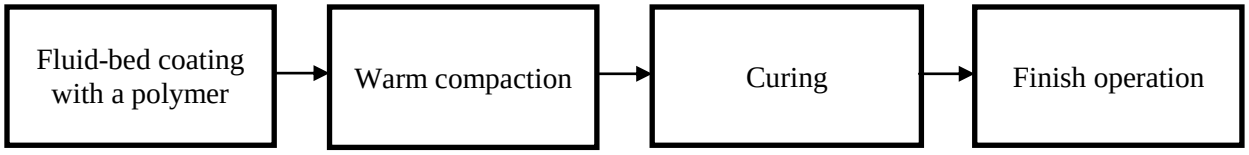

Figure 6. Processing steps in Hoegaenes Company to produce fluid-bed coated iron powder parts [13].

A summary of density and magnetic properties of fluid-bed coated iron powder (with different polymer amount) is shown in Table 2. It shows permeability of coated iron powder is decreased as polymer coating amount is increased. This is due to increase

gap between iron powder and decreased amount of iron loading in system. However, increased coating amount improves stability of the permeability at high frequencies (~ 10 kHz). Fluid-bed coating process offers relatively high strength materials and corrosion resistance from polymer coating. Also, it provides good high frequency magnetic properties. However, operating temperature is limited to 400 ºF (200 ºC) due to polymer coating so defects from pressing cannot be annealed out [13].

Table 2. Density and permeability coated iron with different amount of polymer [13].

Material	Polymer coating (wt %)	Density (g/cm^3) at 690 MPa	Initial relative permeability	Maximum relative permeability
SC100	0.75	7.2	100	400
SC120	0.6	7.3	120	425
SC600	0.25	7.4	140	600

2.2.2 Conventionally Compacted Coating

Conventionally compacted coating process in Figure 7 was developed to overcome problems associated with fluid-bed coating process. The process is mostly similar to fluid-bed coating process, but added a cold compaction method. A cold die set is used and materials undergo curing at 300 ºF (150 ºC) [13]. Also, a warm compact method does not involve in heating powder. It only heats a die set and the powder was filled into a warm die.

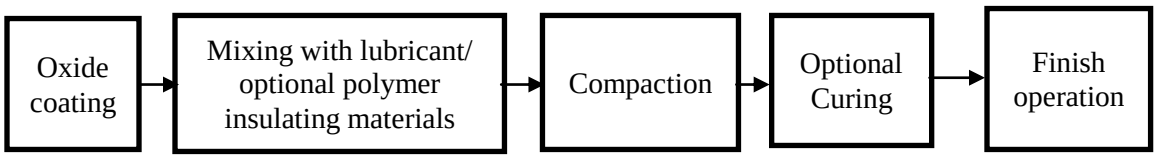

Figure 7. Processing steps to produce conventionally compacted coated iron powder parts with optional polymer insulating materials [13].

Table 3 shows high density for warm compaction compared to that of cold compaction method. However, magnetic properties show that cold compacted material exhibit relative high permeability with low core loss at 60 Hz. The combination of oxide and polymer coating reduces density and permeability of the system due to the increased gap between iron powders [13]. However, presence of oxide coating reduces core loss at high frequency. This is due to high resistivity of oxide coating on surface of iron powder that limits eddy current losses. Limitations of conventionally compacted coating process include low strength and permeability due to the decreased density. However, introducing oxide coating with simple processing steps improves magnetic properties of materials and makes them suitable for static electromagnetic applications.

Table 3. Density, permeability, and core loss depending on compaction method [13].

Compact type	Density (g/cm^3) at 690 MPa	Polymer coating (wt %)	Oxide coating	Initial relative permeability	Maximum relative permeability	Core loss (Wb/lb) at 60 Hz
Cold	7.22	0.5	yes	85	425	0.79
Cold	7.15	0.5	yes	80	230	0.56
Warm	7.45	0.5	yes	90	300	1.38
Warm	7.20	0.5	yes	80	520	2.77

2.2.3 Annealed Coating

Annealed coating process was developed to overcome decreased permeability in conventionally compacted coating process due to low density from oxide coating. Permeability is dependent on not only the density but also the deformation induced by compaction. Annealing to relieve stresses from compaction increases permeability and

decreases hysteresis loss which dominates at low frequency. The process is shown in Figure 8 and is really similar to the two previous methods, but additional annealing step at 1200 ºF (650 ºC) is included [13].

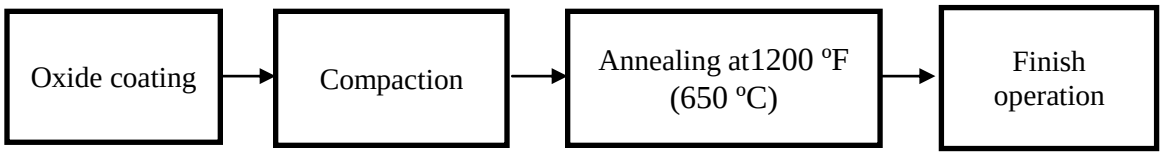

Figure 8. Processing steps for annealed iron powder parts [13].

A summary of magnetic properties for annealed material is shown in Table 4. More insulating coating was processed compared to two previous processes. Density and permeability data is comparable with some of previous materials [13]. Also, it is reported that annealed iron material shows a much smaller hysteresis loop leading to low core loss. However, strength is the main drawback due to the limited strength of the coating material. Hoeganaes recommends this material to use in only applications requiring low core loss.

Table 4. Density and permeability of annealed iron powder parts with 2.0 wt% insulating coating [13].

Material	Insulating coating (wt %)	Density (g/cm^3) at 690 MPa	Initial Permeability	Maximum Permeability
LCM	2.0	7.25	124	245

Since the strength is a main drawback for annealed iron materials in their processes, a new process is developed to produce high density and resistivity materials that can withstand high annealing temperature to increase strength.

2.3 Prior Work

Dr. Patricia Metcalf started this project before the present author. Her initial experiments involved powder coating by sol-gel method, pre-ceramic polymer encapsulation, and electrostatic colloidal deposition. Sol-gel chemistry produces a three dimensional, cross-linked network through hydrolysis and condensation of molecular precursors. The silica sol-gels were synthesized from tetraethoxysilicone (TEOS) and methyltrimethoxysilicone (MTMS) precursors using standard sol-gel processing techniques. A coating of polyvinylpyrrolidone PVP in ethanol was applied prior to depositing the coating to functionalize the surface and increase the adhesion of the sol-gel and silicone coatings to the iron powders [16]. Metal ion dopants were introduced to the sol-gel coatings to produce lower melting glasses [17]. The dopants were also selected to react with the iron powders to produce insulating layers during anneals. The metal dopants tried contained Na, Pb, Bi, and Sn ions. The samples were pressed using a 13 mm diameter, single-acting punch and die set and annealed using 5% hydrogen/95% nitrogen at 900 °C. This was done to try to produce Si_3N_4 in the grain boundaries via the high temperature carbothermal reduction of silica. The resistance of the samples was measured using a simple two probe method. The resistance of the pellets was measured by placing the probes 5 mm apart and measuring the surface

resistance on the face of the pellet. Relative resistance, the ratio of resistance of coated iron to uncoated iron, was only about 1 with relative density of 60-80 % and this is too low for our goal of this project.

The iron particles were then coated with pre-ceramic polymer resins and subsequent to pressing a heat treatment converted the resin into ceramic. Normally pre-ceramic polymers are relatively expensive. However, silicone resin was used since it is cheap and can be converted to silica under the correct conditions. Relative resistance was increased a factor of 20 to 100 but relative density was only about 62 %. The samples were annealed in N_2/H_2 at 500 °C for 15 min. The same die and punch size as used in sol-gel method was used and resistance of the samples was measured under same conditions as sol-gel method resistance measurement procedure.

Dr. Metcalf's experiments for electrostatic colloidal deposition showed promising results using the colloidal coating route. The basis for this process is to coat iron with alumina modified colloidal silica which produces positive zeta potential over a range of slightly basic pH, where the zeta potential of iron is negative. Dr. Metcalf used LUDOX CL, alumina-modified colloidal silica, to create Fe (-)/SiO_2 (+) at pH 8.2, as shown in Figure 9.

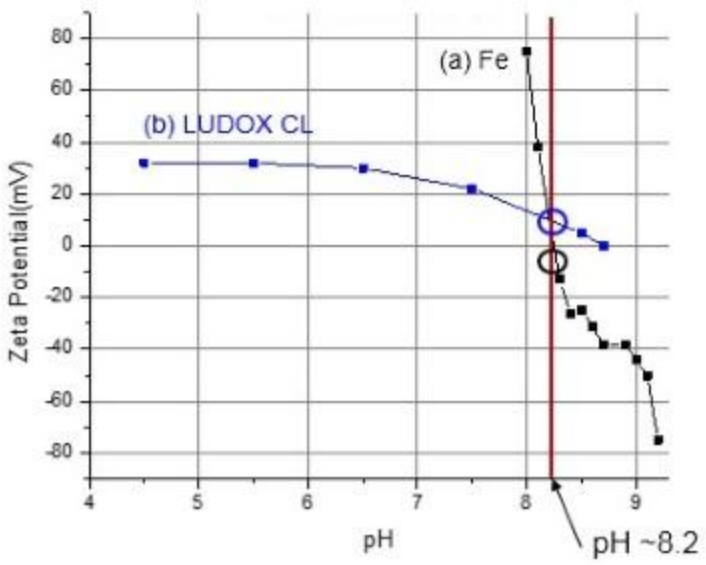

Figure 9. Zeta potential versus pH of (a) iron [18] and (b) LUDOX CL, alumina-modified SiO_2 [19]. This was the basis for producing Fe (-)/SiO_2 (+) at pH~ 8.2.

The samples exhibit bulk resistivity greater than the 10,000 μΩ-cm at the highest relative density of 84 %. The samples were pressed in the wet-coated condition using a 13.5 mm diameter, double-acting punch and die set at 750 MPa. The samples were then fired in a tube furnace in an argon atmosphere containing 5 % hydrogen at 850 °C for 5 h with rate of 10 °C /min. The resistance was measured across the diameter of the samples by contacting copper foils with rubber backing against the sample edge (0.2 cm wide) in a vice. These results provided a sound basis for continuing work on this route.

Before continuing work on this coating route, the starting task was to ensure that the resistivity measurement technique was valid. The samples with the colloidal coating route were used. The HP 34401 multimeter that Dr. Metcalf had used no longer worked. Another meter of the same model, herein referred to as HP 34401 (#2), was located and

used for the repeat measurements to confirm resistivity measurement technique. Comparison of the results using the two meters is shown in Table 5. The repeat measurements are the average of 3 trials on the same location of the specimens, with the uncertainty representing the range of the measured values. Re-measurement using the different meter showed lower resistivity compared to the original measurements, for both the uncoated and coated samples. The relative values between the uncoated and coated samples are consistent, but the absolute values are lower. The reason for these differences is not clear but subsequent measurements with the second meter were consistent and repeatable.

Table 5. Re-measured resistivity of uncoated and colloidal silica coated fine iron powder using different meter.

			Original Measurements using HP 34401(#1)		Re-measured using HP 34401(#2)	
Sample	Green Density (%)	Fired Density (%)	Resistance (μΩ)	Resistivity (min) (μΩ-cm)	Resistance (μΩ)	Resistivity (min) (μΩ-cm)
12-06-002 (uncoated)	89	90	3×10^4	1500	2×10^5	1000 ± 100
12-06-005 (coated)	81	80	6×10^5	35,000	1.5×10^5	8100 ± 400

Based on Dr. Metcalf's promising results on electrostatic colloidal deposition, a series of experiments was conducted to develop the coating process to produce a dry-pressable coated powder with high resistivity (~10,000 μΩ-cm) and density (> 90 %), as required for commercial applications.

CHAPTER 3. EXPERIMENTAL PROCEDURE

3.1 Overview

Dr. Metcalf's experiments were performed in wet-pressed route meaning the coated powder mixture was pressed wet and then dried. Figure 9 shows the zeta potential of iron would be highly sensitive to pH near 8.2, and pH above 8.2 would be necessary to maintain a stable negative iron surface charge. Therefore a series of samples was prepared with pH variations of 8.3 to 8.5 in wet-pressed coating route. The process shifted from wet to dry-pressed coating route as necessary for commercial viability. Dry-pressed coating route means wet mixture was dried in an oven and separated dry particles were pressed in the same double-acting punch and die set. The 2 x 2 study to explore effect of Kenolube and micro-alumina additions was investigated because the original coating route involved direct wet-pressed coating route, so this was the only opportunity to add lubricant. Then, optimization of LUDOX CL coating amount, high shear mixing, and multimodal packing were studied to improve density. LUDOX TM, unmodified colloidal silica, was used instead of LUDOX CL for negatively charged colloidal silica because LUDOX CL only allows to work in a narrow range of pH, close to the isoelectric point (IEP) of both iron and LUDOX CL shown in Figure 9. Such careful control of pH is not

considered like LUDOX CL for LUDOX TM to process Fe (+)/SiO_2 (-). Figure 10 shows optimum selection of pH~8 to provide Fe (+)/SiO_2 (-).

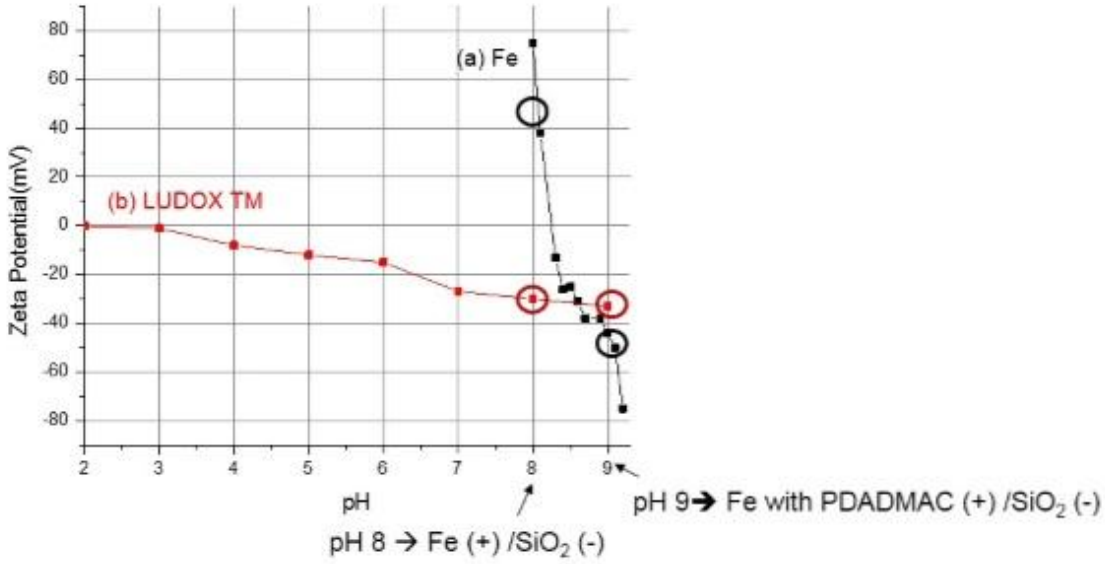

Figure 10. Zeta potential versus pH of Fe (+)/SiO_2 (-) and Fe with PDADMAC (+)/ SiO_2 (-) (a) iron [18], (b) LUDOX TM [20].

A new process was explored with addition of cationic charged electrolyte, polydiallyldimethylammonium chloride (PDADMAC). Figure 10 shows optimum selection of pH ~9 to create Fe with PDADMAC (+)/ SiO_2 (-). Here, the main purpose of using PDADMAC is to provide stronger adhesive for colloidal silica to surface of iron particles unlike previous coating route, shown in Figure 11.

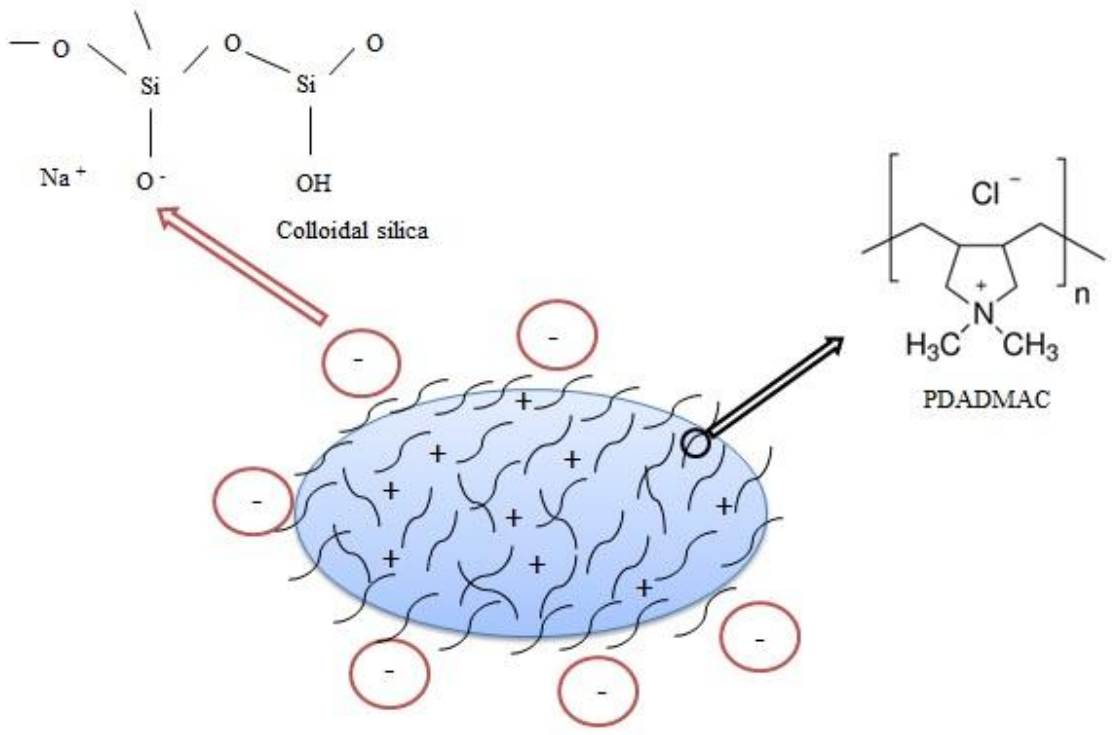

Figure 11. Schematic diagram of unmodified colloidal silica coating with addition of PDADMAC.

3.2 Materials

Coarse and fine iron powder were provided by Hoeganaes Company. Particles size distributions were measured by linear intercept method in optical microscope to be 424 ± 108 μm for coarse and184 ± 40 μm for fine iron powder, shown in Figure 12 (a) and (b).

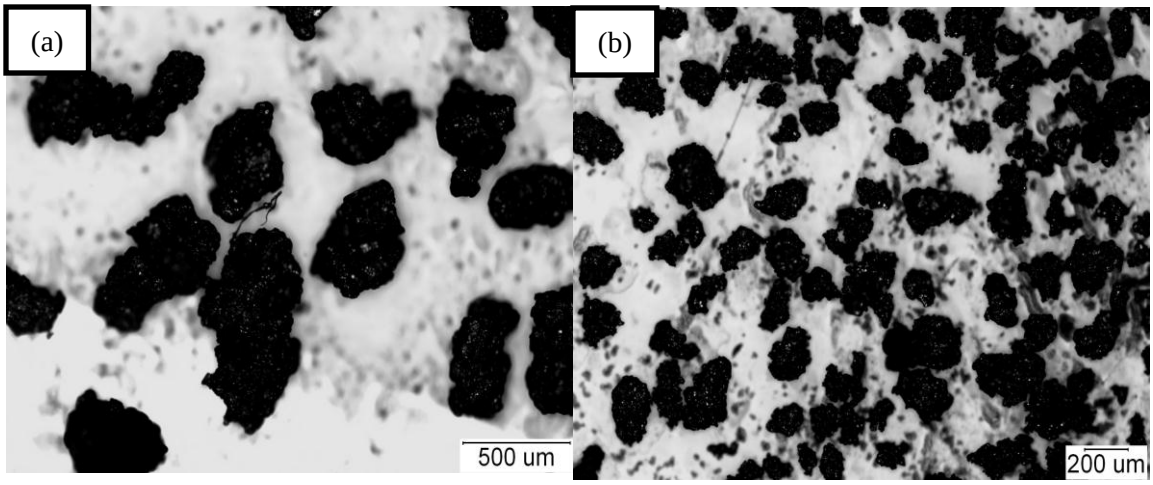

Figure 12. Optical microscope image of (a) coarse iron powder (424 ± 108 µm) (b) fine iron powder (184 ± 40 µm).

LUDOX TM-50 (pH~9), non-modified colloidal silica, was obtained from Sigma-Aldrich. It is a suspension containing 50 wt% silica in H_2O with specific surface area of 140 m^2/g, and 22 nm average particle size. LUDOX CL-30 (pH~4.5), an alumina modified silica, was obtained from Sigma-Aldrich. It is a suspension containing 30 wt% alumina-silica in H_2O with specific surface area of 230 m^2/g, and 22 nm average particle size. Schematic of surface configurations for both LUDOX TM and LUDOX CL are shown in Figure 13 (a) and (b) respectively. These colloidal silica suspensions have been characterized in great detail by Hall [19].

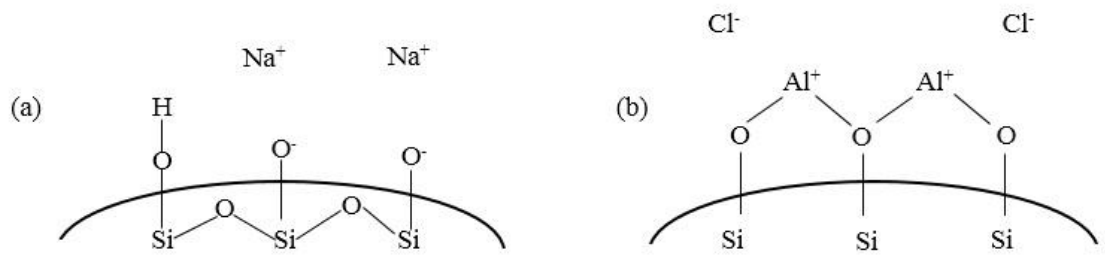

Figure 13. Schematic of surface configurations of (a) unmodified colloidal silica (LUDOX TM) and (b) alumina-modified silica (LUDOX CL). Redrawn from [19].

Kenolube is a composite lubricant supplied by Hoganas AB. It consists of zinc stearate and other wax constituents (2 % Zn as a metal soap) and has average particle size of 27 μm, providing fast flow, and relative high compressibility.

Sumitomo AKP-50 alumina was obtained from Sumitomo Chemical. It is high purity α-alumina (≥ 99.99) with average particle size of 0.2 μm and very narrow size distribution [21].

Poly diallyldimethylammonium chloride (PDADMAC) dispersant solution, shown in Figure 14, was obtained from Sigma-Aldrich. It is a cationic charged electrolyte containing 20 wt% in H_2O with average molecular weight (M_w) of 100,000-200,000 g/mol. It is a water soluble ionic polymer that has a large influence on the stability and the flocculation behavior of suspensions.

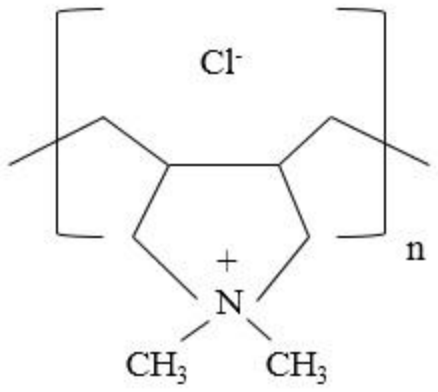

Figure 14. A schematic of PDADMAC dispersant. Redrawn from [22].

3.3 Wet-pressed Coating Route

Original process developed by Dr. Metcalf first involved adding 0.078 g (0.3 wt %) Kenolube to 25 g of the coarse, uncoated iron particles. Then, 0.78 g (3 wt %) of α-Al_2O_3 (0.2 μm Sumitomo AKP-50) was added. The Kenolube and alumina were thoroughly mixed into the powder by hand. Next, 5 mL of aqueous NH_4OH solution of pH 8.4 was added and mixed, followed by 5 mL of LUDOX CL (a viscous suspension). The samples were mixed and the excess liquid was drained off. The damp mixture (5 g) was pressed using a 13.5 mm diameter, double-acting punch and die set at 24,000 lb (=1.07 x 10^5 N), corresponding to a pressing pressure of 750 MPa. The thickness of pellets was approximately 0.32 mm for each 5 g pressed pellet. Then, pellets were dried in an oven at 100 ºC overnight. The samples are fired in a tube furnace in an argon atmosphere containing 5 % hydrogen (flowing ~100 cm^3/min at 1 atm total pressure) at 850 ºC for 5 h with heating and cooling rate of 10 ºC/min. An overall schematic of wet-pressed coating procedure is shown in Figure 15.

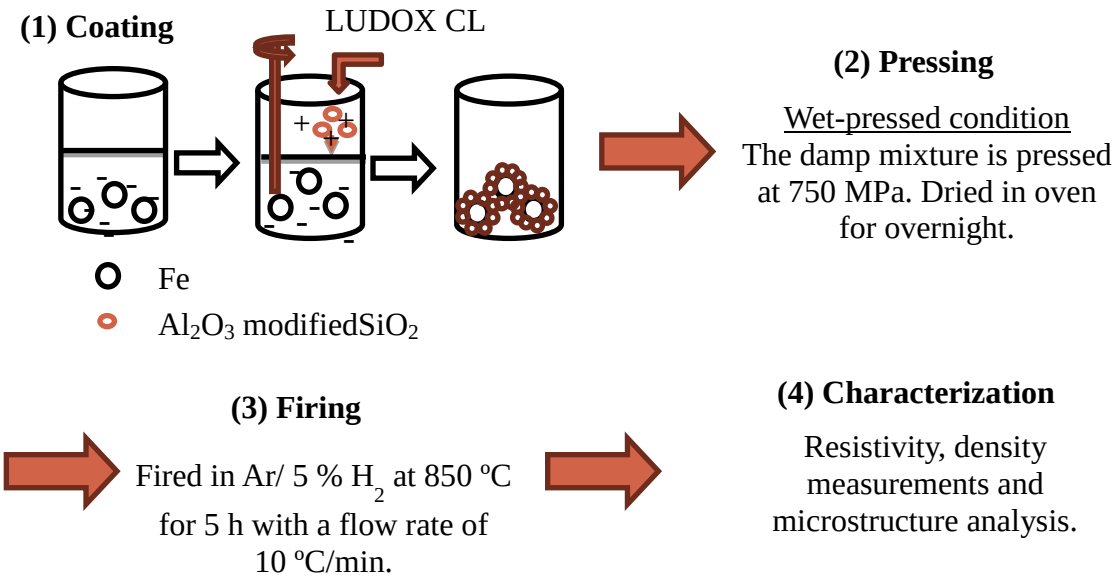

Figure 15. An overall schematic of wet-pressed coating route.

3.4 Dry-pressed Coating Route

In the initial dried coating method the same formulation and procedure as in wet coating method were followed. After draining of excess liquid, coated powders are dried in oven at 100 ºC overnight. Then, the aggregated particles were broken apart by hand. Pressing and firing procedures are performed under same conditions as the wet-pressed procedure. An overall schematic diagram of dry-pressed coating procedure is shown in Figure 16.

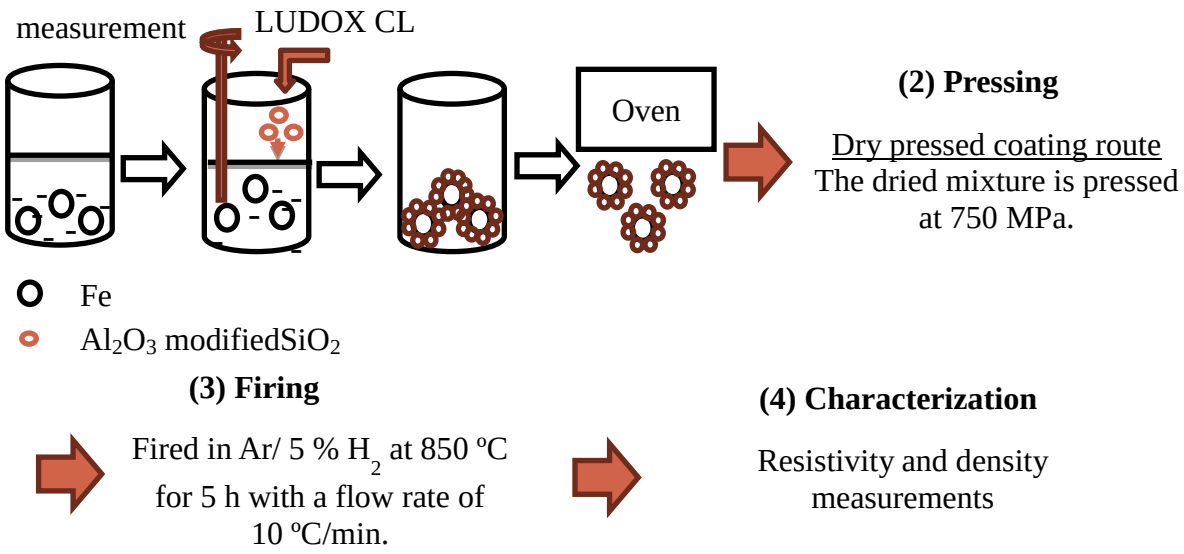

Figure 16. An overall schematic diagram of dry-pressed coating route.

3.5 Additional Process Variables

The 2 x 2 study was explored to investigate effect of Kenolube and micro-alumina. Then, optimization of LUDOX CL coating amount, high shear mixing using coffee grinder, and multimodal packing were studied to increase density. Note that coating procedures of all these studies were performed in dry-pressed coating route except changing in few parameters. The Kenolube/micro-alumina study includes four batches: 1. Kenolube and micro-alumina in coating, 2. No Kenolube, but micro-alumina in coating. 3. Kenolube but no micro-alumina in coating, 4. No Kenolube and no micro-alumina in coating. Optimization of coating amount was studied by systematically reducing LUDOX CL amount from 5 mL down to 1 mL. Grinding as-received coarse and fine iron powders was conducted for 15 to 20 seconds. The time was limited by rapid heating of the powder. After confirming no effect on iron particle size and shape by using the coffee grinder, 0.3

wt % Kenolube was added and mixed in the grinder for 15 to 20 seconds, at three different stages: before coating, after coating, and before and after coating. Both coarse and fine powders were studied. One pellet was pressed and the green density measured for each condition. Based on a simple model shown in Figure 17, a coarse (C): fine (F) blend of 2.7C:1F by volume (equivalent by weight) was selected and the standard dry-pressed coating process were conducted on the mixture.

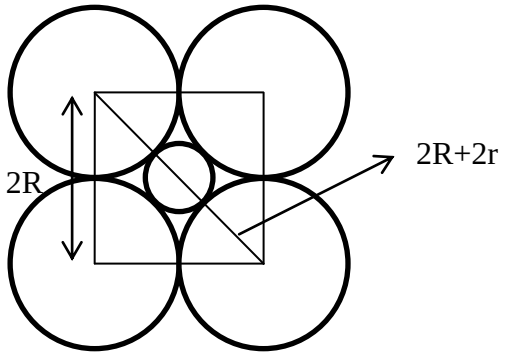

R= radius of coarse iron particle
r= radius of fine iron particle

Figure 17**.** A schematic of simple packing model for multimodal packing (2.7C:1F by volume).

3.6 LUDOX TM Dry-pressed Coating Route and Addition of PDADMAC Study

The main difference using LUDOX TM compared to LUDOX CL is to create positively charged surface iron particles with negative unmodified colloidal silica (Fe (+)/SiO_2 (-)), shown in Figure 10. Coating procedure of LUDOX TM dry-pressed route (without addition of PDADMAC) is same as dry-pressed coating route except using slightly lower pH of NH_4OH solutions (pH ~8) and less amount of LUDOX TM (3 mL).

Each batch for LUDOX TM-50 coating route with addition of PDADMAC was prepared in 25 g of both fine and coarse uncoated iron particles for addition of PDADMAC study. Next, 10 mL of an aqueous NH_4OH solution with a pH ≅ 9 was added, and ~0.1 g of PDADMAC was added for both fine and coarse batch. The mixture was thoroughly mixed with spatchula. Then, excess liquid was drained off. The damp powder was washed with 80 mL pH ≅ 9 adjusted water in 10 mL increments each time. This was done because excess amount of PDADMAC present in solution creates agglomeration of silica suspensions. Then, 10 mL of an aqueous NH_4OH solution with a pH ≅ 9 was added again. Next, 3 mL of LUDOX TM was added to samples. Separate batches with less amount of LUDOX TM (1 and 0.3 mL) were prepared to increase density. Pressing and firing procedures were performed under same condition as LUDOX CL coating route. An overall schematic of this coating route is shown in Figure 18.

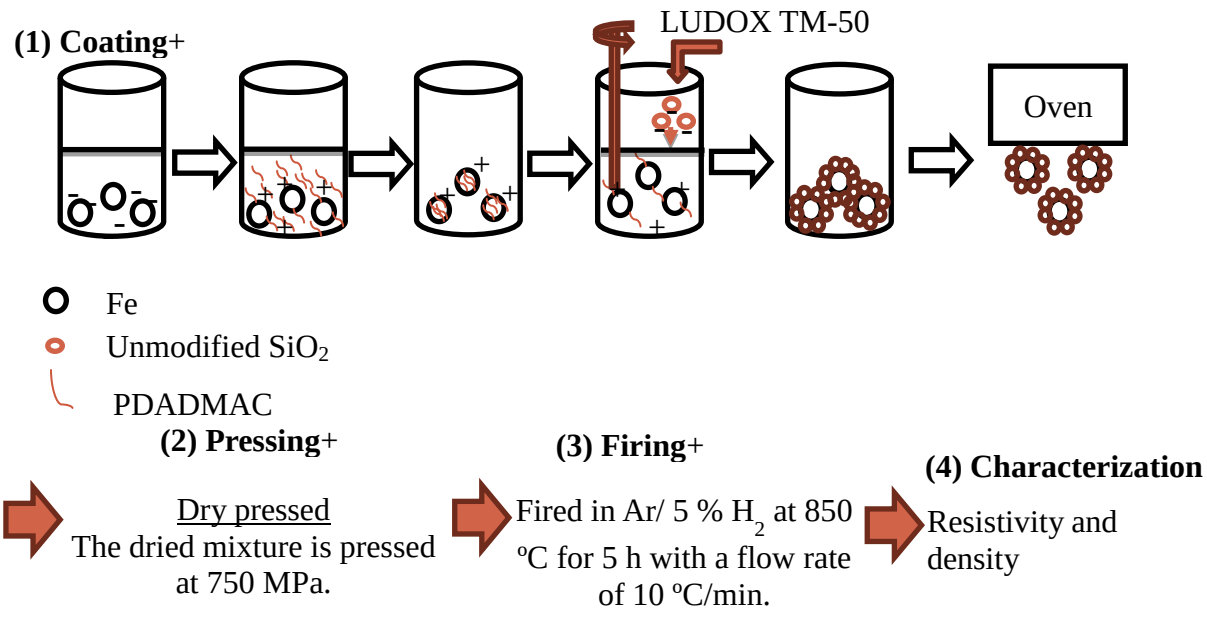

Figure 18. An overall schematic of LUDOX TM + PDADMAC coating route.

3.7 Resistivity and Microstructure Characterization

Electrical resistance was measured across the diameter of the pellets. The edges of the specimens were lightly ground with fine abrasive paper and opposed contacts across the diameter were made to the pellets by clamping copper foils with rubber backing against the pellet edges in a vice. The compression of the rubber caused the foils to contact the pellets along 0.2 cm of the specimen edge, as measured with the pellets in the vice. The resistivity was estimated assuming a uniform cross-sectional area of conduction equal to the contact width, w (= 0.2 cm), times the pellet thickness, t, shown in Figure 19. This area corresponds to the minimum cross-sectional area for conduction, and thus gives the lower bound of resistivity, whereas the effective conduction area is a larger, but unknown, value less than the pellet diameter times thickness.

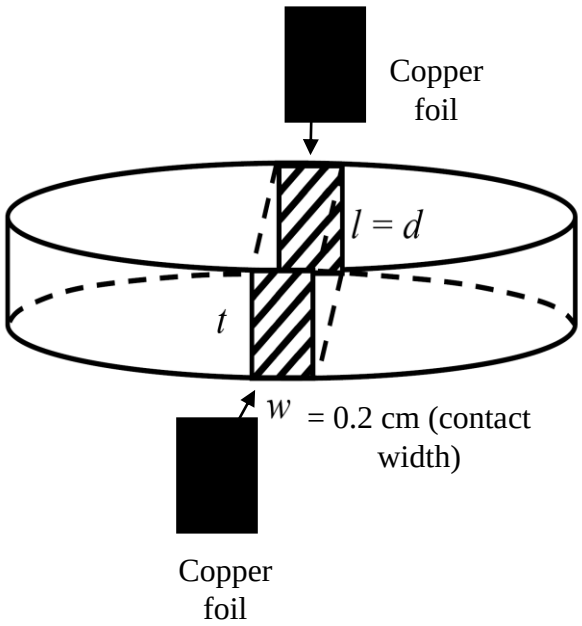

Figure 19. A schematic of resistance measurement across the diameter that creates contact width of 0.2 cm by clamping copper foils with rubber backing against the pellet edges.

The resistivity was then calculated as, $\rho = R (A/L)$, where L is the average diameter of the pellets, A is the cross-sectional area and R is the measured resistance. Average of three trials on the same location of the specimens was measured.

Epoxy resins were used for mounting porous materials so that they are penetrated through pores to prevent pullouts. Grinding was carried out with 320, 400, 600 SiC grits for about 90 sec, 90 sec, and 3 min respectively, followed by polishing Then, they were polished with diamond paste (6 and 3 μm) and finally with alumina suspension (0.05 μm). Nikon optical microscope was used to investigate particle shape and size. Detailed microstructure of LUDOX coated iron was studied.

Scanning electron microscope was used to study presence of coating. Desired sample was placed on SEM sample holder using carbon tape. Images were taken at different magnification and composition of phases was studied by EDS.

CHAPTER 4. RESULTS AND DISCUSSIONS

4.1 Wet-pressed Coating Route

The first results in wet-pressed coating route exhibit resistivity greater than the 10,000 μΩ-cm, but highest relative density of only 84 %. Dr. Metcalf used pH 8.2 to create Fe (-)/SiO_2 (+). Zeta potential data for iron shown in Figure 9 suggested the zeta potential would be highly sensitive to pH near 8.2 and pH above 8.2 would be necessary to maintain a stable negative surface charge. Therefore a series of samples was prepared by wet-pressed coating method with pH variations of 8.3 to 8.5. The finer iron powder was also replaced by the coarser powder in an attempt to increase the density. The finer powder is subject to agglomeration effects and they resist deformation due to more contact points per unit volume. Also, hysteresis and eddy current losses depend on particle size [6]. Increasing particle size is known to decrease coercive force, but eddy current loss is proportional to particle size squared so there is a trade-off between these two losses [6]. Here, effects of particle size on hysteresis and eddy current losses are not studied, but they can be investigated after obtaining desired density and resistivity measurements. Therefore, coarse iron powder is used in most subsequent experiments, except where noted. The resulting density and resistivity values are shown in Table 6. The average of two samples is reported. The higher relative density of 88 % compared to

the original experiment (Table 5) was obtained most likely from less agglomeration of the coarser powder. There are no significant trends in density or resistivity with the variation in pH in this range. Although the resistivity is a little lower, the coating is still effective considering both that higher density and lower surface area with the larger particle size would each tend to decrease resistivity. These values are 0.5 to 0.7 of the target resistivity, and still higher relative density must be obtained.

Table 6. Average density and resistivity values (± range/2) for colloidal coated (coarse Fe) samples prepared at different pH values (wet-pressed).

Sample	Green Density (%)	Fired Density (%)	Resistance (μΩ)	Resistivity (min) (μΩ-cm)
pH 8.3	88	89	1.4×10^5	7000 ± 1200
pH 8.4	87	87	1.5×10^5	7300 ± 1000
pH 8.5	87	89	1.0×10^5	5200 ± 1400

To investigate density and possible coating evidence, optical microstructure images were taken for the pH 8.4 sample, shown in Figure 20. Unlike the uncoated sample (91 %, 1400 μΩ-cm), the coated sample clearly shows separation between particles. This is expected due to coating presence between the iron particles. Density measured from systematic point count method (from image) and direct physical measurement (mass and volume) showed essentially no difference.

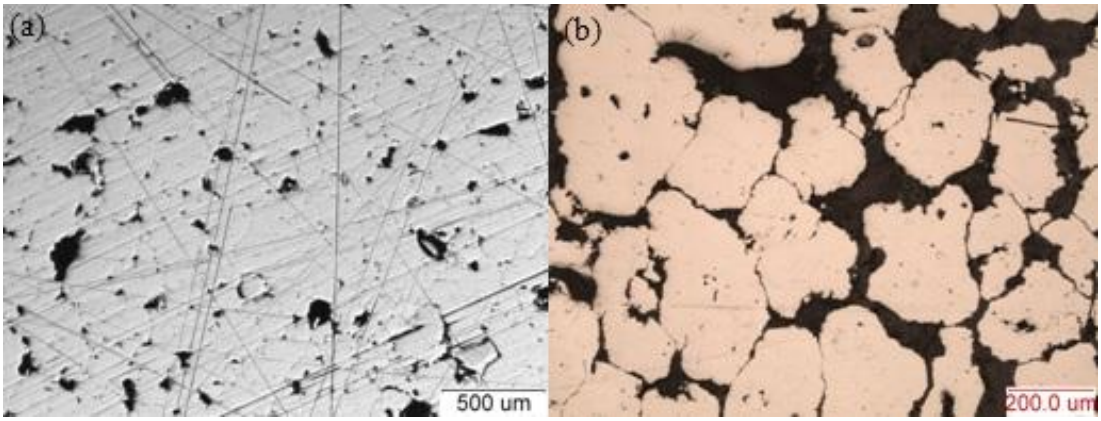

Figure 20. Optical microscope images of wet-pressed coating route with pH 8.4 (a) uncoated and (b) coated.

SEM-EDS of the wet-pressed pH 8.4 samples was conducted to investigate more details of microstructural reasons for the density and resistivity in wet-pressed coating route. Figure 21 shows the wet-pressed pellet surface. At low magnification (a) shows the iron particles are clearly visible. At higher magnification (b) shows a relatively thick, fine particulate layer is apparent between the iron particles. EDS measurements on both iron particles and the region between them are shown in (c) and (d). The analyses clearly show high Si, Al, and O contents between the iron particles (c), proving the presence of coating and a strong iron signal from the particles (d). The layer is cracked in a way that typically occurs from shrinkage during drying (or perhaps also firing)

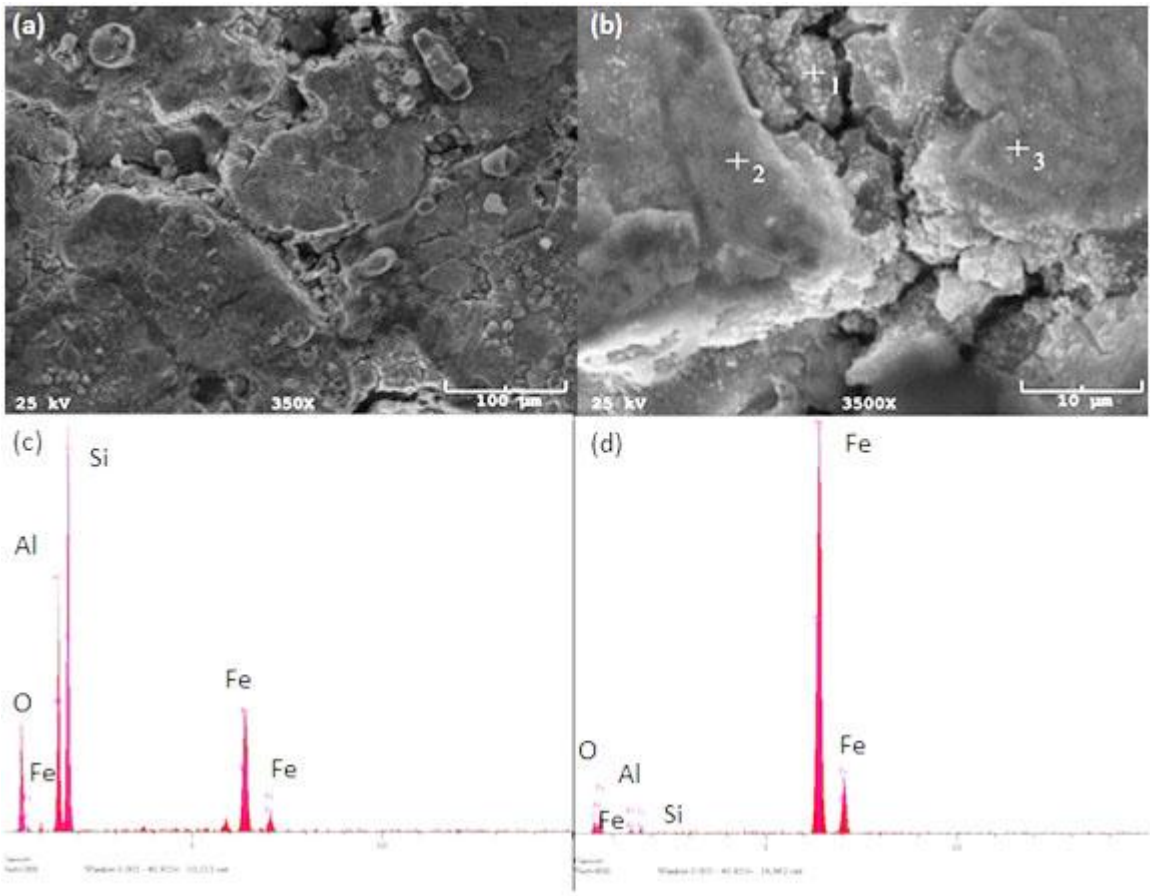

Figure 21. SEM at (a) low and (b) high magnification of wet-pressed fired pellet surface. EDS microanalysis at (c) point 1 and (d) point 2 in image (b) is consistent with the coating between the iron particles.

4.2 Dry-pressed Coating Route

The wet-pressed coating route demonstrated the effectiveness of the colloidal coating, but in order to be commercially viable the coated powder is required to be pressable in a dry condition. The key results shown in Table 7 is a ~100-fold increase in resistivity compared to the wet-pressing coating route, with only a small decrease in density. There is no physical basis to expect that the 3 to 4 times higher resistivity at pH

8.4 is due to the pH differences of only one-tenth point. The average value of 860,000 μΩ-cm for the three different pH values is thus taken as representative in this range, which is on the order of 100 times the target value of 10,000 μΩ-cm.

Table 7. Average density and resistivity values (± range/2) for colloidal coated (dried coating and dry-pressed) samples prepared at different pH values.

Sample	Green Density (%)	Fired Density (%)	Resistance (μΩ)	Resistivity (min) (μΩ-cm)
pH 8.3	85	87	8.6×10^6	420,000 ± 68,000
pH 8.4	84	85	3.3×10^7	1,600,000 ± 220,000
pH 8.5	85	87	1.2×10^7	570,000 ± 24,000

To investigate the coating further, optical microscope images were taken as shown in Figure 22. Comparing between uncoated (90 %, 1200 μΩ-cm) and coated (pH 8.4 sample in Table 7) samples, (a) and (b) clearly show separation between particles for coated sample. Epoxy resin was injected onto surface of samples to distinguish between powder coating and porosity in the samples. Images (c) and (d) show clear separation between coating on iron surface and epoxy resin, thus proving coating presence.

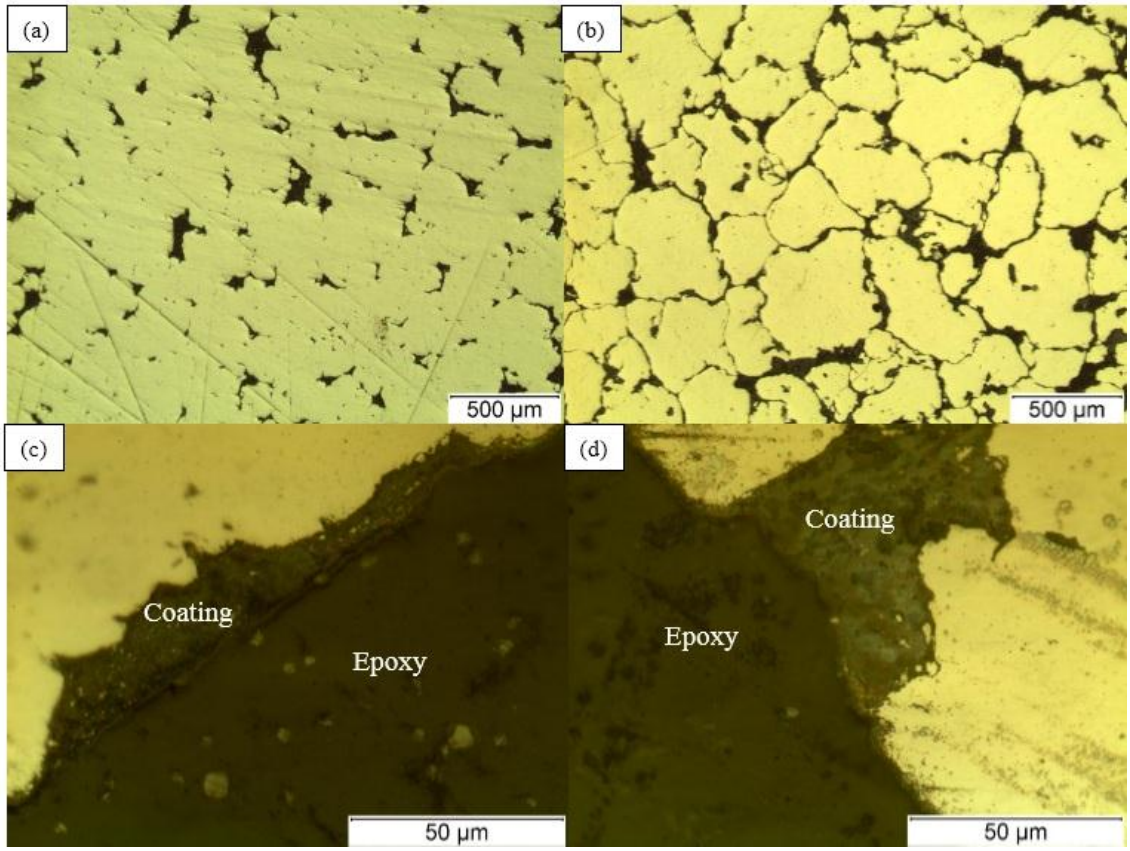

Figure 22. Optical microscope images of (a) uncoated, (b) dry coated sample after firing. Higher magnification images (c) and (d) show separation between particles and clear boundary for coating and epoxy resin proving coating presence.

SEM images of the dry pressed pellet surface are shown in Figure 23. Analysis by EDS at high magnification suggests a thin coating rich in Si and containing Al on the surface of the iron particles in some regions. The thickness of the layer was difficult to clearly resolve, but appeared in several regions to be ~2 µm.

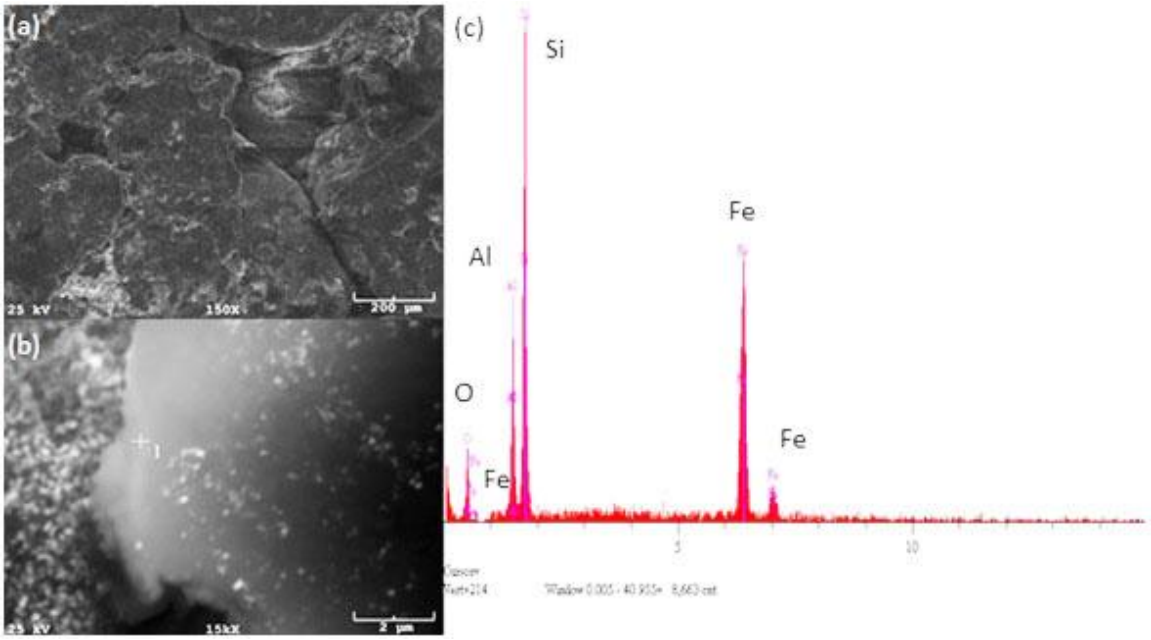

Figure 23. SEM images at (a) low and (b) high magnification (same field as (a)) of dry pressed pellet surface showing coating thickness of ~2 µm. (c) EDS composition spectrum at point 1 in (b) showing high content of silica and alumina.

Unlike wet-pressed coating route, dry-pressed coating route does not show cracks in insulating layer after pressing and firing. The resistivity differences are most likely due to differences in the coating since the density values were nearly the same, although slightly lower density of dry-pressed is consistent with higher resistivity. Also, likely in wet-pressed coating route the wet coating gets pushed out between particles allowing more contacts of iron particles. The micro-alumina particulate (Sumitomo AKP-50, 0.2 µm) and lubricant (Kenolube) additions are also variables that could affect the process. The micro-alumina was originally added in earlier work on silicone-based polymer coating in an attempt to inhibit Fe particle contact during pressing. The amount added, 3 wt % of the iron, corresponds to about 6 vol. % of the iron-alumina mixture. A small

amount of Kenolube was also added from the beginning of the colloidal coating process development. Although such lubricant is normally added to aid pressing of dry powders by lubricating moving surfaces (particle-particle and particle-die), the original colloidal coating route involved direct wet pressing, so this was the only opportunity to add lubricant. Whether the lubricant has the desired effect after going through the wet processing or plays a role in the coating process itself were not known at this point. Therefore, a 2 x 2 study was conducted to explore the separate, and possibly interactive, effects of these two variables. The results are compared in Tables 8. Overall, only small effects on the green and fired density are noted, but very large effects on resistivity occurred. Removing the micro-alumina from the coating process (keeping the Kenolube) decreased resistivity from 860,000 to 18,000 μΩ-cm, which is still about twice the target value. However, removing the Kenolube from the coating process (but adding 0.3 wt % to the dry coated powder before pressing), with or without the alumina, resulted in larger loss of resistivity to 1700 and 600 μΩ-cm, respectively. These results suggest a critical role of the Kenolube in the coating process itself.

Table 8. Density and resistivity for the conditions with and without micro-alumina and Kenolube additions in the coating process.

Green Density (%)	Fired Density (%)	Resistance (μΩ)	Resistivity (μΩ-cm)	Green Density (%)	Fired Density (%)	Resistance (μΩ)	Resistivity (μΩ-cm)
3 wt% alumina							
0.3 wt.% Kenolube before coating				No Kenolube in coating*			
84	85	2.4×10^8	860,000	83	83	3.3×10^4	1700
No alumina							
0.3 wt.% Kenolube before coating				No Kenolube in coating*			
83	84	1.7×10^5	18,000	86	88	2.1×10^4	600

*0.3 wt% Kenolube added to dry coated powder before pressing.

Kenolube is a so-called composite lubricant, consisting of zinc stearate and other wax constituents (2% Zn) [23]. To investigate the effect of both Kenolube and micro-alumina, the influence of pH was studied first. Here, the same proportion of pH-adjusted water to coarse iron powder as used earlier was not possible because the iron powder was limited. However, adding 25 g iron powder in 20 mL of pH ~8.4 water increased pH from 8.4 to 8.6 due to formation of hydroxide group on iron surface. In dry-pressed coating route, 5 mL of pH ~8.4 water was added in 25 g of iron powder so pH of 5 mL solution containing 25 g iron powder was expected to be higher due to greater ratio between iron powder and water. Therefore, 20 mL of pH ~8.4 water was added instead of 5 mL because sufficient water was required to measure pH. Next, 0.3 wt % Kenolube and 3 wt % micro-alumina were added just like dry-pressed coating route and they resulted in decreasing pH from 8.6 to 8.25. Kenolube and micro-alumina were added individually to study which one was the major component decreasing pH of solution. Kenolube had the most effect, decreasing pH of the solution (from 8.6 to 8.3) and adding micro-alumina had only small effect (from 8.6 to 8.55). Adding Kenolube can stabilize pH of the solution to produce Fe (-) / modified SiO_2 (+).

However, this pH investigation does not fully explain the effect of the micro-alumina since it has small influence on pH of solution. Therefore, zeta potential vs. pH of the micro-alumina was obtained and isoelectric point (IEP) was at about pH 8.7, shown in Figure 24. This proves that micro-alumina particles have positively charged surfaces at pH ~ 8.4 and they can adhere to negatively charged iron surface. Alumina is widely known as insulating materials (10^{13} to 10^{15} Ω-cm resistivity at 20 °C) so it has an intrinsic effect in increasing resistivity also [24].

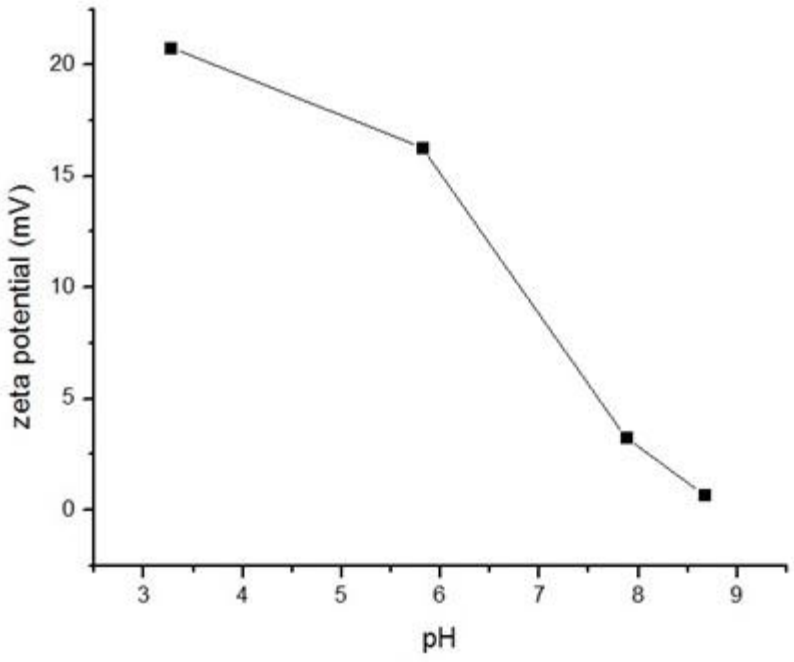

Figure 24. Zeta potential vs. pH of micro-alumina (AKP-50) showing isoelectric point (IEP) at about 8.7.

The exact composition of Kenolube is unknown, but contains zinc stearate and other wax constituents (2 % Zn as a metal soap). Presence of zinc metal can have an effect in increasing resistivity. Between pH ~7 and 13, ZnO or $Zn(OH)_2$ is the stable form according to the Pourbaix diagram, shown in Figure 25, and isoelectric point of $Zn(OH)_2$ is known to be about 10.3 [25].

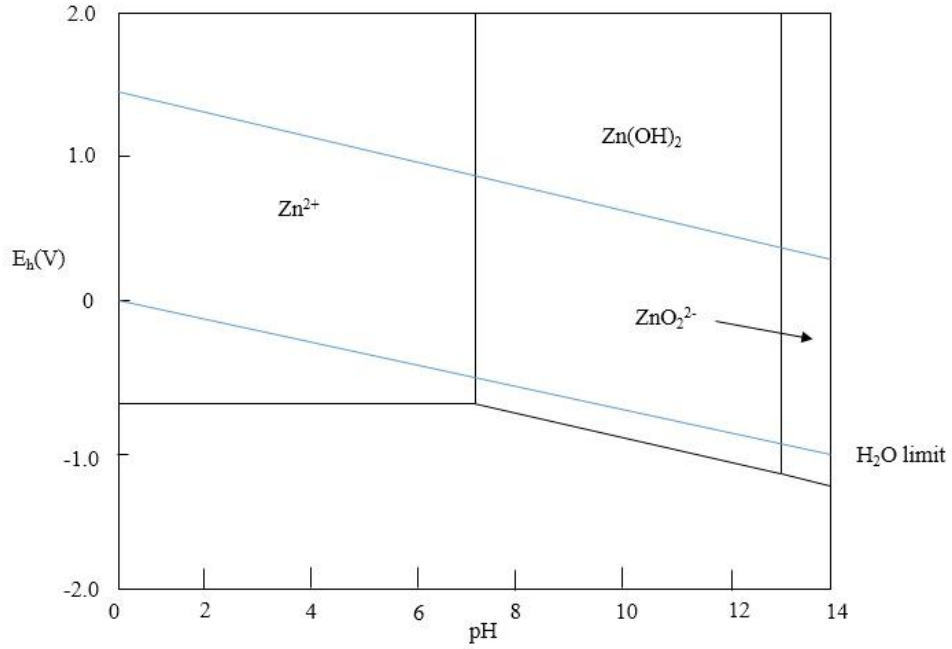

Figure 25. Pourbaix diagram of Zn-H_2O system at 25 °C. Redrawn from [26].

At pH 8.4, positively charged Zn surface is created and most likely it will not interact with micro-alumina since both of them have same charges. Positively charged zinc hydroxide can also adhere to negatively charged iron surface. Numerous studies indicate that ZnO can have high resistivity depending on its form and preparation method that creates intrinsic or extrinsic defects. Bulk ZnO is known to have resistivity between 1 and 10 Ω-cm [27]. Resistivity of prepared ZnO thin films is in order of 1500 Ω-cm [28]. Also, 99.998 % purity ZnO shows 0.75 M Ω-m at room temperature [29]. Only a small amount of Zn is present in Kenolube but high resistivity can result in enhancing resistivity in the system.

On the basis that the dry-pressed coating route was providing much greater resistivity than necessary (~100 times) an attempt at reducing the coating thickness in order to increase the density was undertaken. The amount of LUDOX CL was systematically reduced from 5 mL down to 1 mL, per 25 g Fe, to increase density by providing a thinner coating. The results in Table 9 show a strong dependence of the resistivity on the amount of LUDOX CL in these experiments. Reducing the LUDOX CL only 10 % dropped the resistivity by over two orders of magnitude, with further decreases plateauing to ~1000 μΩ-cm. With decreasing LUDOX CL addition the density increased, up to ~90%, consistent with a reduction in agglomeration effects. Although the amount of colloidal silica available for the coating decreases with decreasing addition, another important difference may have been the effective pH, as the amount of pH-adjusted water was held constant at 5 mL per 25 g Fe. Therefore, with less colloidal SiO_2 suspension added (natural pH ~4.5) the higher relative amount of pH 8.4 water would drive the pH up, reducing the zeta potential (Figure 9). The apparent marked rise in resistivity between 4.0 and 5.0 mL LUDOX CL suggests a critical pH effect of this type.

Table 9. Density and resistivity values of uncoated and dry coated samples made with 5.0 to 1.0 mL LUDOX-CL per 25 g coarse Fe.

Sample (mL of LUDOX CL)	Green Density (%)	Fired Density (%)	Resistance (μΩ)	Resistivity (μΩ-cm)
Uncoated	89	90	20,000	1000
5.0	84	85	3.3×10^7	1,600,000
4.5	85	85	885,000	44,000
4.0	87	87	59,000	2850
3.5	86	87	33,000	1550
3.0	91	91	18,500	850
1.0	91	90	14,000	700

A coffee grinder was used in an attempt to provide better mixing of lubricant with iron powder. First, a study was conducted to determine the effect of the grinder on the as-received coarse and fine iron powders by grinding for 15 to 20 seconds. The time was limited by rapid heating of the powder. Figure 26 shows the optical micrographs of the powders before and after grinding. Particle size distributions were measured using optical microscopy software. As-received coarse powder had an average particle size (± std dev) of 424 ± 108 μm and after grinding 486 ± 80 μm. The as-received fine powder showed a size of 184 ± 40 μm and after grinding 178 ± 29 μm. Measurements prove that the coffee grinder did not significantly affect the particle size distributions. The micrographs do show there is a significant effect of smoothing (burnishing) the particle surfaces, especially in the coarse powder, which suggests that the coating would have to adhere well to the iron surfaces in order to not be damaged by the grinding process used for mixing in the lubricant.

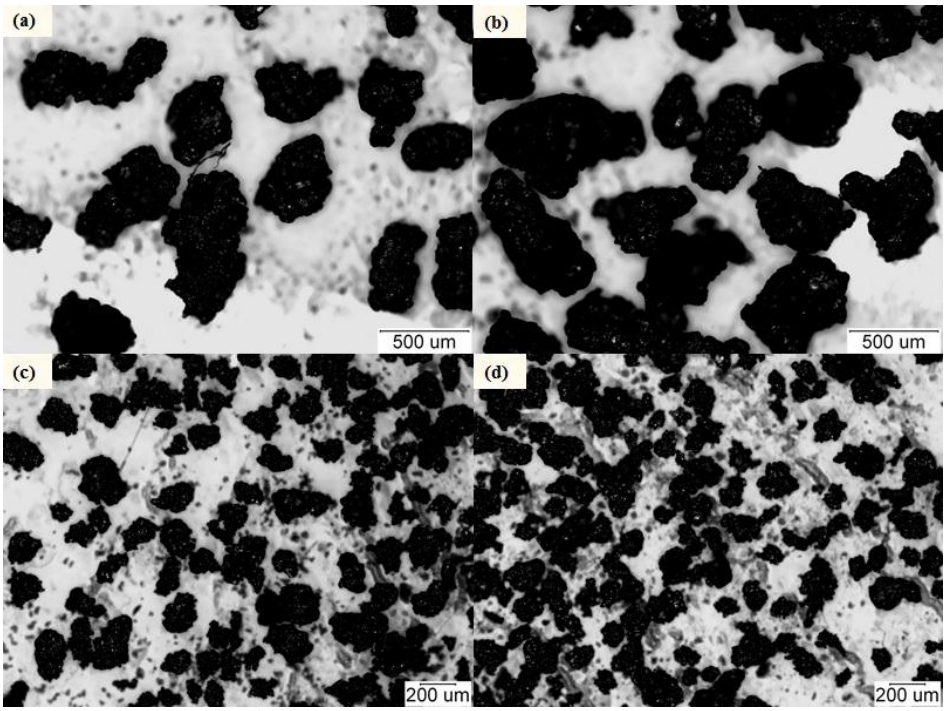

Figure 26 (a) As-received coarse powder (b) ground coarse powder (c) as-received fine powder (d) ground fine powder.

After confirming no effect on iron particle size and shape by using the coffee grinder, 0.3 wt% Kenolube was added and mixed in the grinder for 15 to 20 seconds, at three different stages: before coating, after coating, and before and after coating. Both the coarse and fine powder were studied. The purpose of adding lubricants is to facilitate particle rearrangement and reduce friction forces from the die in pressing. One pellet was pressed and the green density measured for each condition.

Measured green densities are shown in Table 10. The uncoated (coarse) sample showed high density (94%), with perhaps a slight increase in green density by adding 0.3 wt% Kenolube. For coated coarse samples the stage at which lubricant was added had no effect on the green density and the density values were lower than for mixing the

lubricant by hand. For coated fine samples, there also was essentially no effect of lubricant addition stage on green density and the values were even lower compared to the coarse powder. These results suggest the lubricant addition by the high-shear mixing had little if any benefit for pressing. This indicates that mixing by hand with a spatchula provides enough mixing of iron powder, Kenolube, and micro-alumina.

Table 10. Effect on green density of pressed coarse and fine powder, uncoated and dry coated with Kenolube before (0.3 wt %), after (0.3 wt %) and before and after (0.6 wt % total) coating.

Sample	Green Density (%)
Uncoated	
Coarse, without Kenolube	94
Coarse, with Kenolube	95
Coated	
Coarse, Kenolube before coating	80
Coarse, Kenolube after coating	80
Coarse, Kenolube before and after coating	80
Fine, Kenolube before coating	77
Fine, Kenolube after coating	75
Fine, Kenolube before and after coating	76

Multimodal powder was explored to improve the density of the dry coated processes, blending the fine and coarse powders for multimodal packing effects. Based on a simple packing model, a coarse:fine blend of 2.7C:1F by volume (equivalent by weight) was selected and the standard dry coating process conducted on the mixture. However, this gave densities about the same as for the all-coarse powder, ~85%, but much lower resistivity of only ~ 2000 μΩ-cm. Perhaps blending uncoated powder with the coated powder up to the random packing percolation limit (~16%) would provide

higher density without loss of resistivity. Calculation of coarse to fine proportions was based on spherical shape of iron particles but they have such an irregular shape so it may not have provided optimum estimation of fine powder amount.

4.3 LUDOX TM Dry-pressed Coating Route and Addition of PDADMAC

LUDOX TM, unmodified colloidal silica, was used instead of LUDOX CL for negatively charged colloidal silica because LUDOX CL only allows to work in a narrow range of pH, close to isoelectric point (IEP) of both iron and LUDOX CL, shown in Figure 9. Such careful control of pH is not necessary for LUDOX TM to achieve Fe (+)/SiO_2 (-) as shown in Figure 10.

Table 11 shows density and resistivity measurement of LUDOX TM (3 mL) dry-pressed coating route without addition of PDADMAC. Relative density of 78 % and resistivity of 120,000 μΩ-cm were obtained. Like LUDOX CL dry-pressed coating route, optical microscope images were taken to investigate presence of coating on iron particles to prove high resistivity measurements. Figure 27 (a) and (b) clearly show comparison between uncoated and coated sample with reducing metal-metal contact between particles.

Epoxy resin was employed onto surface of coated sample just like LUDOX CL and Figure 27 (c) shows clear boundary between coating and epoxy. This is consistent with LUDOX CL optical microscope images in Figure 22.

Table 11. Density and resistivity measurement of LUDOX TM dry-pressed coating route.

Sample	Green Density (%)	Fired Density (%)	Resistance (μΩ)	Resistivity (μΩ-cm)
pH 8	78	78	2.5×10^{6}	120,000

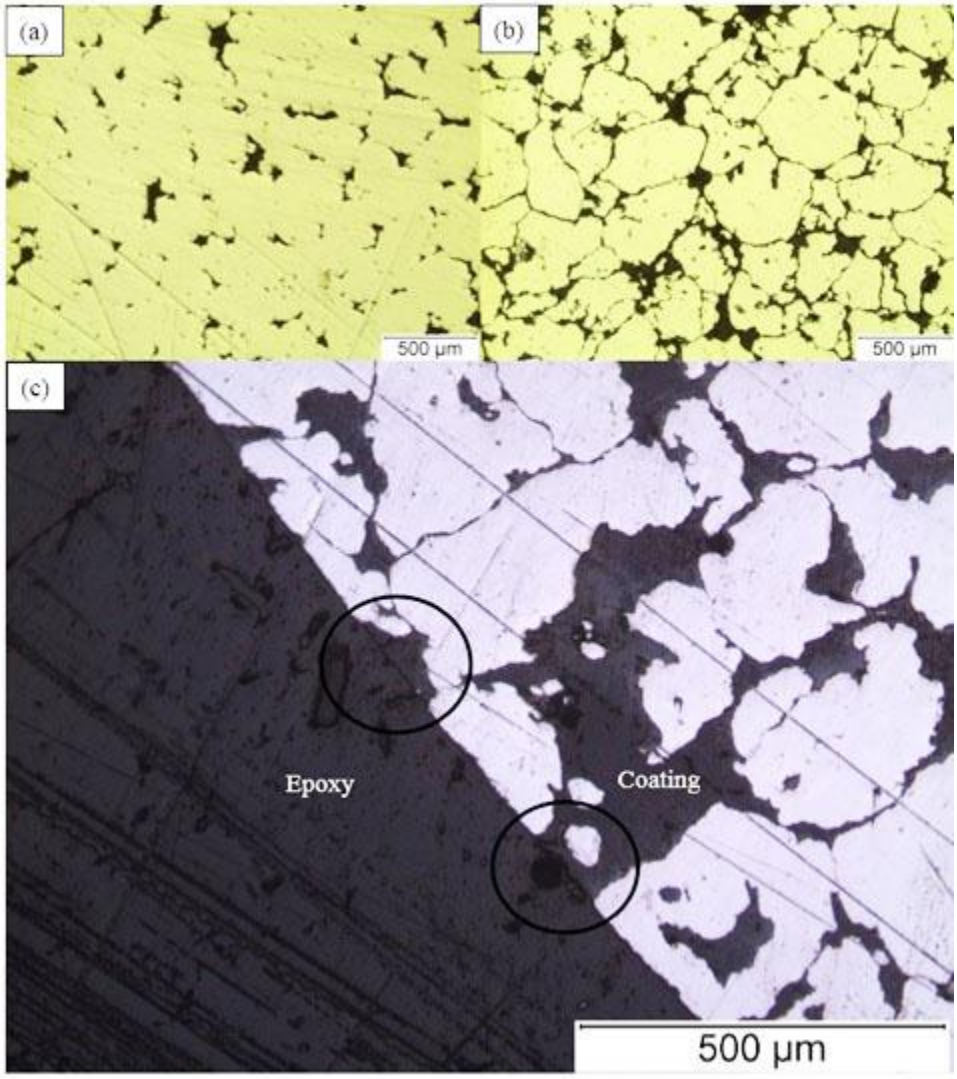

Figure 27. Optical microscope images of (a) uncoated (90 %, 1400 μΩ-cm) (b), (c) coated showing clear separation of iron particles and coating presence in epoxy resin.

Addition of PDADMAC was tried with the idea it provides stronger adhesive for colloidal silica to surface of iron particles, unlike previous LUDOX TM-50 dry-pressed coating route. Table 12 shows relative density and resistivity before and after firing. The average of two samples is reported. The density of the uncoated sample was 90 % and that of the coated was 89 % for the coarse powder while coated fine powder samples had 87 %. The higher density values most likely resulted from less agglomeration of the coarser powder. This was the highest density obtained of all coated samples. Resistivity was about 50 times higher than that of the uncoated samples.

Table 12. Average density and resistivity for LUDOX TM-50 (with PDADMAC) coated and uncoated samples.

Sample	Green Density (%)	Fired Density (%)	Resistivity before firing(μΩ-cm)	Resistivity after firing(μΩ-cm)
Uncoated				
Coarse	91	91	NA	1600
Coated				
Coarse	88	89	39,000	49,000
Fine	86	87	52,000	51,000

The next step was to check repeatability. However, results in Table 13 showed that resistivity was approximately the same compared to the uncoated sample in Table 12. Also, a decrease in density (1~2 %) was obtained. One possible hypothesis regarding this problem was due to contamination of the furnace since mineral oil was back-flowed by mistake when repeated processing was performed. Mineral oil is composed of mostly hydrocarbons. This could have made more reducing atmosphere in the furnace. The reason why the repeated experiment gave lower resistivity after firing in Table 13 is

uncertain at this point. However, it was believed that contamination from previous users can play a critical role

Table 13. Average density and resistivity for repeated LUDOX TM-50 (with PDADMAC) coated samples.

Sample	Green Density (%)	Fired Density (%)	Resistivity before firing(μΩ-cm)	Resistivity after firing(μΩ-cm)
Coarse	86	86	38,000	<1500
Fine	85	85	55,000	<1500

An important observation was made while polishing both high- and low-resistivity specimens to compare microstructure. As explained in the procedure section, the edges of the specimens were lightly ground with fine abrasive paper to measure resistance. This is to remove oxidation on the surface. However, it was found that the edges of the samples having high resistivity after firing were not fully removed. Fine abrasive was not enough to fully remove the oxidation. The reason why repeated samples had thinner layer of oxidation is possibly because of hydrocarbons from mineral oil, which makes reducing atmosphere in the furnace. After fully removing the oxide from the original samples by grinding more, the re-measured resistivity was consistent with the lower value of repeated samples. This result suggest possible furnace atmosphere differences were not the source of the resistivity difference. Instead, the PDADMAC itself may be the difference.

Coating with smaller amount of LUDOX TM-50 (0.3 and 1 mL) with PDADMAC was attempted to increase density because the first experiment with PDADMAC coating

route showed high resistivity (Table 12). Thin layer of silica coating can lead to higher packing density. Table 14 shows the density and resistivity before and after firing. There was an increase in density while resistivity before firing was sufficient to meet the target the value, but the fired resistivity again was low. This suggests that PDADMAC may play a role on decreasing fired resistivity.

Table 14. Density and resistivity for repeated colloidal coated samples with less amount of LUDOX TM-50.

Sample	Green Density (%)	Fired Density (%)	Resistivity before firing(μΩ-cm)	Resistivity after firing(μΩ-cm)
Coarse-0.3 mL	90	90	16,000	<1500
Coarse-1 mL	93	92	6,000	<1500
Fine-0.3 mL	91	91	12,000	<1500
Fine-1 mL	91	91	8,800	<1500

CHAPTER 5. SUMMARY

The main goal of this project was to develop a commercially viable coating of iron powders for press-and-sinter processing that would enable higher firing temperatures to anneal out magnetic defects, while maintaining high electrical resistivity (~10,000 μΩ-cm) and high density (> 90 %). Electrostatic colloidal deposition showed promising results in earlier experiments, exhibiting bulk resistivity greater than the 10,000 μΩ-cm at the highest density of 84 %. This route was developed further in this study.

A series of samples was prepared with pH variations of 8.3 to 8.5 for wet-pressed coating route because recent zeta potential data for iron suggested the zeta potential would be highly sensitive to pH near 8.2. The average resistivity of 6500 ± 1100 μΩ-cm and density of 88 ± 1 % are reported because there were no significant differences with respect to pH between 8.3 and 8.5.

The wet-pressed coating method demonstrated the effectiveness of the colloidal coating, but in order to be commercially viable, the powder had to be pressable in a dry condition. About 100-fold increase in resistivity compared to the wet-pressing route was obtained, with only a small decrease in density (1-2 %). The average value of 860,000 μΩ-cm is reported for dry-pressed coating method at pH 8.4.

Removing the micro-alumina from the coating process (keeping the Kenolube) decreased resistivity from 860,000 to 18,000 μΩ-cm, which is still about twice the target value. However, removing the Kenolube from the coating process (but adding 0.3 wt % to the dry coated powder before pressing), with or without the alumina, resulted in larger loss of resistivity to 1700 and 600 μΩ-cm, respectively. This result confirmed that Kenolube has an effect on stabilizing pH of the solution and presence of Zn metal can have an effect on resistivity since ZnO is the stable form at pH 8.4 and exhibits positively charged surface. Also, micro-alumina exhibit positively charged surface and they can adhere to surface of iron at pH 8.4.

Optimization of LUDOX CL amount, high shear mixing, and multimodal packing were studied to increase density since much higher than necessary resistivity measurements were obtained throughout the study. Reducing the Ludox CL only 10 % dropped the resistivity by over two orders of magnitude, with further decreases plateauing to ~1000 μΩ-cm. With decreasing Ludox CL addition the density increased, up to ~90 %, consistent with a reduction in agglomeration effects. High shear mixing of the uncoated (coarse) sample showed high density (94 %), with perhaps a slight increase in green density by adding 0.3 wt % Kenolube. For coated coarse samples the stage at which lubricant was added had no effect on the green density and the density values were lower than for mixing the lubricant by hand. For coated fine samples, there also was essentially no effect of lubricant addition stage on green density and the values were even lower compared to the coarse powder. These results suggest the lubricant addition by the high-shear mixing had little if any benefit for pressing. Based on a simple packing model, a coarse:fine blend of 2.7C:1F by volume (equivalent by weight) was selected and the

standard dry coating process conducted on the mixture. However, this gave densities about the same as for the all-coarse powder, ~85 %, but much lower resistivity of only ~ 2000.

LUDOX TM coating route to provide Fe (+)/SiO_2 (-) were studied and it showed relative density of 78 % and resistivity of 120,000 μΩ-cm were obtained. Microstructure analysis clearly showed separation between particles and clear boundary between coating and epoxy proving coating presence.

LUDOX TM coating route (3 mL) with PDADMAC showed the highest density of 89 % for the coated coarse powder and of 87 % for fine powder. However, resistivity of both coarse and fine coated samples showed less than 1500 μΩ-cm after firing. There were possible furnace atmosphere differences, but they were not the source of the resistivity difference. Instead, the PDADMAC itself may be the difference. Reducing amount of LUDOX TM from 3 mL to 1mL for the coarse powder showed the highest density of 92 %. There was an increase in density while resistivity before firing was sufficient to meet the target the value, but the fired resistivity again was low. This suggests that PDADMAC may play a role on decreasing fired resistivity. This is a promising result to improve density but resistivity need to be improved.

REFERENCES

REFERENCES

[1] M.D. Fenton, Iron and Steel, U.S. Geological Survey, Mineral Commodity Summaries, February 2014

[2] R. M. German, Powder Metallurgy of Iron and Steel, John Wiley and Sons, Inc., New York, 1998.

[3] Z. Ye, "Modelling and experimental analysis of core losses of SMC components" Hoganas AB, SE-263 83, Sweden (2014).

[4] C.W. Chen, Magnetism and Metallurgy of Soft Magnetic Materials, North-Holland Publishing Company, New York, 1977.

[5] F.G. Hanejko, G.W. Ellis, T.J. Hale, "Application of high performance material processing electromagnetic products" Hoeganaes Corporation, PM2TEC'98 (2008).

[6] E. Tombacz, A. Majzik, ZS. Horvat, E. Illes, “Magnetite in aqueous medium: coating its surface and surface coated with it.” *Romanian Reports in Physics*, **58** 281-286 (2006).

[7] T. Madeda, H. Toyoda, N. Igarashi, K. Hirose, K. Mimura, T. Nishioka, A. Ikegaya, "Development of super low iron-loss P/M soft magnetic materials" *SEI Technical Review*, **60** 3-9 (2005).

[8] W. D. Callister, Jr, Materials Science and Engineering: An Introduction, John Wiley and Sons, Inc., New York, 2007.

[9] R. Boll, Soft Magnetic Materials: fundamentals, alloys, properties, products, applications, Heyden and Son Ltd, London, 1978.

[10] A. Nussbaum, Electronic and Magnetic Behavior of Materials, Prentice-Hall,Inc., Englewood Cliffs, New Jersey, 1967.

[11] K. Narasimhan, F. Hanejko, M. L. Marucci, "Soft magnetic material for A.C. applications" Hoeganaes Corporation.

[12] H. Hojo, N. Akagi, T. Sawayama, H. Mitani, "Newly developed iron powder for highly efficient dust cores" *Kobelco Technology Review*, **30** 30-35 (2011).

[13] M. L. Marucci, K. S. Narasimhan, "Advances, applications, and opportunities for coated iron powder for electromagnetic applications" Hoeganaes Corporation, PM2TEC03 (2003).

[14] V. Saini, "Fluidized bed processing for multiparticulates" *J. Chem*., **2** (2) 447-450 (2009).

[15] S. Srivastava, G. Mishra, "Fluid bed technology: overview and parameters for processing selection" *International J. of Pharmaceutical Sciences and Drug Research*, **2** (4) 236-246 (2010).

[16] Y. Leng, K. Sato, J. Li, *Powder Technol*ogy, 196 80-84 (2009).

[17] P. Rao, M. Reddy, K. Sudhakar, and N. Veeraiah, *Philosophical Magazine* **88(11)** 1601-1615 (2008); B. Chaudhuri, K. Chaudhuri, and K. Som, *J Phys.Chem. Solids*, **50** 1149-1155 (1989); M. Karabulut, E. Melnik., *J. Noncryst. Solids*, **288** 8-17 (2001); S. Mandal and A. Ghosh, *J Chem Phys*, **106** (15) 6310-6313 (1997).

[18] Y. P. Sun, X. Li, J. Cao, W. Zhang, and H. Wang, "Characterization of zero-valent iron nanoparticles", *Adv Colloid Interface Sci*, **120** 47-56 (2006).

[19] C. A. Hall, "Deposition of aluminum oxide modified core-shell silica particles onto Silica Surfaces" MS Thesis, University of Manchester (2010).

[20] G. Orts-Gil, K. Natte, D. Dresche, "Characterisation of silica nanoparticles prior to in vitro studies: form primary particles to agglomerates" *J. Nanopart. Res*, **13** 1593-1604 (2011).

[21] S. Fujiwara, Y. Tamura, H. Maki, N. Azuma, Y. Takeuchi, "Development of new high-purity alumina" Sumitomo Kagaku 2007-I.

[22] D. Bauer, E. Killmann, W. Jaeger, "Adsorption of poly (diallyl-dimethylammoniumchloride) (PDADMAC) and of copolymers of DADMAC with N-methyl-N-vinyl-acetamide (NMVA) on colloidal silica" *Colloid Polym. Sci*, **109** 161-169 (1998).

[23] A. Bergkvist, "Stainless steel powders for high density applications" S-263 83, Hoganas, Sweden.

[24] L. Pawloski, "The relationship between structure and dielectric properties in plasma-sprayed alumina coatings" *Surface and coatings technology*, **35** 285-298 (1988).

[25] R. Marsalek, "Particle size and zeta potential of ZnO" *APCBEE Procedia*, **9** 13-17 (2014).

[26] A. T. Al-Hinai, M. H. Al-Hinai, J. Dutta, "Application of E_h-pH diagram for room temperature precipitation of zinc stannate microcubes in an aqueous media" Material *Research Bulletin*, **49** 645-650 (2014).

[27] E. Ziegler, A. Heinrich, H. Oppermann, G. Stover, *Phys. Status Solidi*, **66** 635 (1981).

[28] F.R. Blom, F. C. M. Pol, G. Bauhuis, T. J. A. Popma, *Thin Solid Films*, **204** 365 (1991).

[29] T. K. Roy, D. Sanyal, D. Bhowmich, A. Chakrabarti, "Temperature dependent resistivity study on zinc oxide and the role of defects" *Materials Science in Semiconductor Processing*, **16** 332-336 (2013).